Retrieval Algorithm for Aerosol Effective Height from the Geostationary Environment Monitoring Spectrometer (GEMS)

Sang Seo Park[1,*], Jhoon Kim[2], Yeseul Cho[2], Hanlim Lee[3], Junsung Park[3], Dong-Won Lee[4], Won-Jin Lee[4], Deok-Rae Kim[4]

[1] *Department of Urban and Environmental Engineering, Ulsan National Institute of Science and Technology, Ulsan, Korea*

[2]*Department of Atmospheric Sciences, Yonsei University, Seoul, Korea*

[3]*Division of Earth and Environmental System Sciences, Pukyong National University, Busan, South Korea*

[4]*Envionment Satellite Center, National Institute of Environmental Research, Incheon, Korea*

[*]Corresponding author. Sang Seo Park (sangseopark@unist.ac.kr)

Submitted to Atmospheric Measurement Techniques

2023. 06.

Abstract

An algorithm for aerosol effective height (AEH) was developed for operational use with observations from the Geostationary Environment Monitoring Spectrometer (GEMS). The retrieval technique uses the slant column density of the oxygen dimer (O_2-O_2) at 477 nm, which is converted into AEH after retrieval of aerosol and surface optical properties from GEMS operational algorithms. The AEH retrieval results show significant AEH values and continuously monitor aerosol vertical height information in severe dust plumes over East Asia, and the collection of plume height information for anthropogenic aerosol pollutants over India. Compared to the AEH retrieved from Cloud-Aerosol Lidar with Orthogonal Polarization (CALIOP), the retrieval results show insignificant bias with a standard deviation of 1.4 km for the AEH difference over the GEMS observation domain from January to June 2021 due to uncertainty in input parameters for aerosol and surface. The AEH difference depends on aerosol optical properties and surface albedo. Compared to the aerosol layer height obtained from the tropospheric monitoring instrument (TROPOMI), differences of 0.78 ± 0.81 and 1.16 ± 0.92 km were obtained for pixels with single scattering albedo (SSA) < 0.90 and 0.90 < SSA < 0.95, respectively, with significant dependence on aerosol type.

Keywords: aerosol effective height, aerosol optical depth, environmental satellite, GEMS

1. Introduction

Since the launch of the Total Ozone Mapping Spectrometer (TOMS) on Nimbus-7, ultraviolet (UV)-visible satellite measurements have been used for environmental monitoring of the distribution and reaction processes of pollutants (e.g., anthropogenic aerosols, tropospheric ozone, NO_2, and SO_2). Measurements from environmental satellites have been used to estimate gaseous species in the atmosphere, resulting in vertical column integrated amounts. However, these column-integrated amounts and associated surface concentrations have uncertainty due to simultaneous changes in optical path length associated with the vertical distribution of target species and amounts of scattering materials (clouds and aerosols) present.

~~For this reason, e~~Environmental satellite sensors, in particular those that measure UV-visible wavelength range, have been used to ~~retrieve~~ detect aerosol and cloud signals by using the aerosol index~~to determine aerosol index~~ (e.g., Buchard *et al.*, 2015; Herman *et al.*, 1997; Torres *et al.*, 1998, 2002; Prospero *et al.*, 2000; de Graaf *et al.*, 2005) and scattering radiative index values (Penning de Vries *et al.*, 2009, 2015; Kooreman *et al.*, 2020; Kim *et al.*, 2018), although these indices only have qualitative characteristics and limitations to identify aerosol amounts. In addition, measurements of scattering material amounts, such as aerosol optical depth (AOD) ~~in UV wavelengths~~ and radiative cloud fraction ~~amounts~~, have also been retrieved from pixel-based radiance data in UV-visible wavelength range. Recently, various aerosol retrieval algorithms have been developed for use with satellite sensors. These algorithms focus on improved trace gas retrieval as well as direct monitoring of aerosol properties, such as AOD and single scattering albedo (SSA) (e.g., Ahn *et al.*, 2014; Kim *et al.*, 2020; Torres et al., 2020).

Although the algorithms developed for environmental satellite sensors indicate the

presence and amount of scattering materials, the accuracy of these retrieval algorithms for trace gases is significantly affected by the relative vertical distributions between trace gases and scattering materials (e.g., Lorente *et al.*, 2017; Hong *et al.*, 2017). For this reason, estimating cloud and aerosol vertical parameters is very important. For cloud vertical information, cloud height information has been estimated simultaneously with cloud optical depth and radiative cloud fraction data using the rotational Raman scattering (Joiner and Vasilkov, 2006; Vasilkov *et al.*, 2008; Joiner and Bhartia, 1995) and absorption intensity of the oxygen dimer (O_2-O_2) (Accarreta *et al.*, 2004; Vasilkov *et al.*, 2018; Choi *et al.*, 2021) combined with normalized radiance.

~~For cloud vertical information, cloud height information has been estimated simultaneously with cloud optical depth and radiative cloud fraction data using the rotational Raman scattering (Joiner and Vasilkov, 2006; Vasilkov *et al.*, 2008; Joiner and Bhartia, 1995) and absorption intensity of the oxygen dimer (O_2-O_2) (Accarreta *et al.*, 2004; Vasilkov *et al.*, 2018; Choi *et al.*, 2021) combined with normalized radiance. Because most of cloud optical depth is thick, vertical information of cloud can be accurately determined.~~ Similarly, the aerosol vertical distribution can be estimated using the oxygen~~-related~~ absorption bands, such as the O_2-O_2 (Park *et al.*, 2016; Chimot *et al.*, 2017; Choi *et al.*, 2019, 2020), O_2-A (Dubisson *et al.*, 2009; Geddes and Boesch, 2015; Sanders *et al.*, 2015; Zeng *et al.*, 2020), and O_2-B (~~Chen *et al.*, 2021;~~ Ding *et al.*, 2016) bands, as well as combinations of these bands (Sanghavi *et al.*, 2012; Chen et al., 2021). In addition, an algorithm for aerosol vertical information has been developed based on hyperspectral UV-visible radiance from satellite observation. Nanda *et al.* (2018) demonstrated the possibility of aerosol height retrieval from the O_2-A band developed an algorithm using Tropospheric Monitoring Instrument (TROPOMI)

(Sanders and de Haan, 2016; Nanda *et al.*, 2020) and implemented the algorithm operationally.

However, the vertical distribution of aerosol is difficult to assess because of its large spatio-temporal variability. Although the Cloud-Aerosol Lidar with Orthogonal Polarization (CALIOP) provided the aerosol vertical distribution with high vertical resolution (Omar et al., 2009), other satellites for passive sensors are only able to estimate the representative parameter of aerosol height. Veihelmann et al. (2007) showed that the number of degrees of freedom of signal for aerosol is 2~4 for most of satellite observation conditions by the ozone monitoring instrument (OMI). It means that the number of information for aerosol vertical distribution have a limitation. Because of limitation for describing the aerosol vertical information, aerosol layer height (ALH) (Nanda et al., 2018) or aerosol effective height (AEH) (Park et al., 2016) were defined to retrieve the aerosol vertical information from the passive satellite sensors.

~~However, the vertical distribution of aerosol is more difficult to assess than that of clouds, as the optical properties of aerosols in the atmosphere differ among aerosol types.~~

~~Recently, various aerosol retrieval algorithms have been developed for use with satellite sensors. These algorithms focus on improved trace gas retrieval as well as direct monitoring of aerosol properties. For this reason, AOD and other aerosol optical properties, such as single scattering albedo (SSA), are retrieved from the observed radiance (e.g., Ahn *et al.*, 2014; Kim *et al.*, 2020; Torres et al., 2020). In addition, an algorithm for aerosol vertical information has been developed based on hyperspectral UV-visible radiance from satellite observation. Nanda *et al.* (2018) demonstrated the~~

~~possibility of aerosol height retrieval from the O_2-A band developed an algorithm using Tropospheric Monitoring Instrument (TROPOMI) (Sanders and de Haan, 2016; Nanda *et al.*, 2020).~~

The Geostationary Environment Monitoring Spectrometer (GEMS), which was launched by South Korea in February 2020, retrieves data related to major trace gases and aerosol properties (Kim *et al.*, 2020). The main purpose of GEMS is to monitor air quality, and aerosol properties are targets of such monitoring over East Asia. For this reason, the GEMS aerosol algorithm was developed as multiple operational products. Aerosol properties are obtained for the purposes of monitoring surface air quality and aerosol effects for the air mass factor (AMF) calculation. In addition to the aerosol optical property algorithm, the GEMS aerosol product is additionally applied to the aerosol vertical information, AEH. For the possibility for development of an AEH retrieval algorithm, Park *et al.* (2016) conducted theoretical sensitivity testing of AEH retrieval using solely the O_2-O_2 absorption band along with aerosol and surface properties. Overall, the sensitivity of AEH retrieval was strongly affected by SSA, AOD, and aerosol types including optical and size properties, and the error budget for AEH retrieval using the O_2-O_2 band was 739 ~ 1276 m. In addition, case studies of AEH during dust transport over East Asia were conducted using radiance data from the Ozone Monitoring Instrument (OMI) and aerosol optical properties from the Moderate Resolution Imaging Spectroradiometer (MODIS).

~~In addition to the aerosol optical property algorithm, the standard product of aerosol is additionally applied to the aerosol vertical information, aerosol effective height (AEH).~~

~~For the possibility for development of an AEH retrieval algorithm, Park *et al.* (2016)~~

~~conducted theoretical sensitivity testing of AEH retrieval using solely the O_2-O_2 absorption band along with aerosol and surface properties. Overall, the sensitivity of AEH retrieval was strongly affected by SSA, AOD, and aerosol types including optical and size properties, and the error budget for AEH retrieval using the O_2-O_2 band was 739 ~ 1276 m. In addition, case studies of AEH during dust transport over East Asia were conducted using radiance data from the Ozone Monitoring Instrument (OMI) and aerosol optical properties from the Moderate Resolution Imaging Spectroradiometer (MODIS).~~

Based on theoretical considerations and case results of previous studies, we introduce an operational retrieval algorithm for AEH. Section 2 describes the details of the AEH retrieval algorithm for GEMS and provides a list of the detailed input parameters. Section 3 introduces the details of satellite sensors for the comparison and validation in this study. Section 4 reports retrieval results based on case studies of aerosol transport, and section 5 contains validation results based on Cloud-Aerosol Lidar with Orthogonal Polarization (CALIOP) and TROPOMI data. Finally, we show conclusion and summary in section 6.

2. AEH retrieval algorithm

AEH is a layer height parameter that considers the penetration of photons into the aerosol layer. In this study, the AEH product from GEMS is defined as the height with aerosol extinction integrated from the surface of $(1\text{-}\exp^{-1})$ × AOD, and ~~A~~a detailed definition of AEH was introduced by Park *et al.* (2016). Numerous previous studies have used the aerosol top layer height (Kohkanovsky and Rozanov, 2010) or middle layer height (i.e. ALH) (e.g., Sanders *et al.*, 2015; Nanda *et al.*, 2020) as the aerosol

vertical layer parameter. ~~However, the definition of AEH requires that the altitude region for aerosol extinction be integrated from the surface to (1-exp^{-1}) × AOD. Therefore,~~ AEH is similar to the aerosol top layer height but with a slight bias. For AEH retrieval, the vertical distribution assumption is also important. The Gaussian Density Fitting (GDF) distribution, which is a modified Gaussian distribution structure, is assumed for AEH retrieval. The full-width at half-maximum (FWHM) of the aerosol layer is 1 km. Based on the assumptions about the aerosol vertical distribution, the AEH value is greater than the peak height of the Gaussian distribution and lower than the aerosol top layer height. Detailed description of AEH and other aerosol vertical parameters are shown in Figure 1.

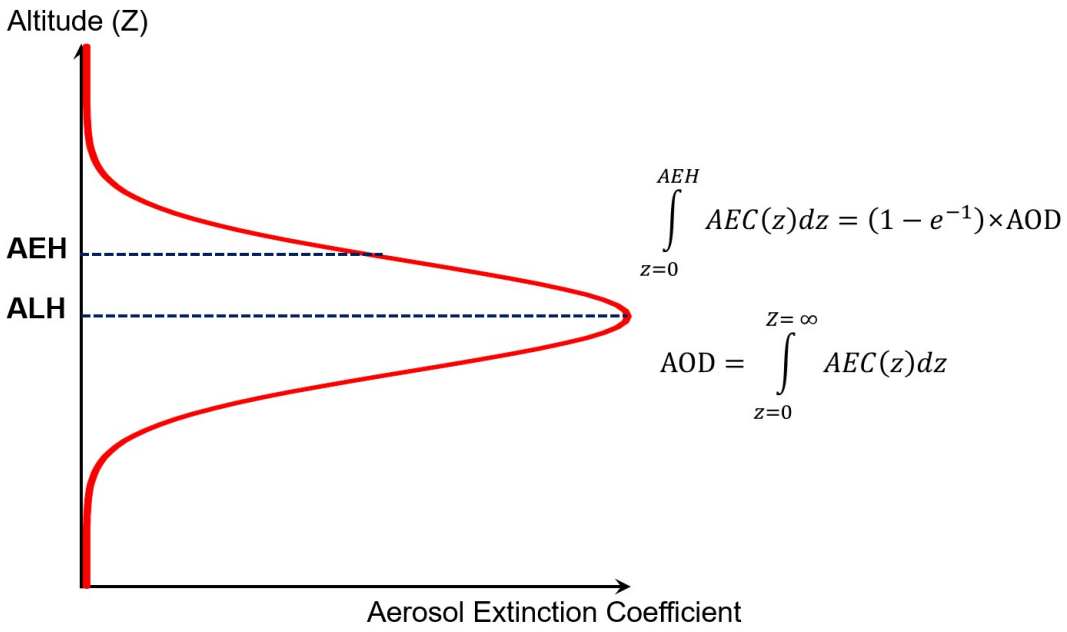

Figure 1. Description of difference between AEH and ALH in idealized aerosol vertical distribution.

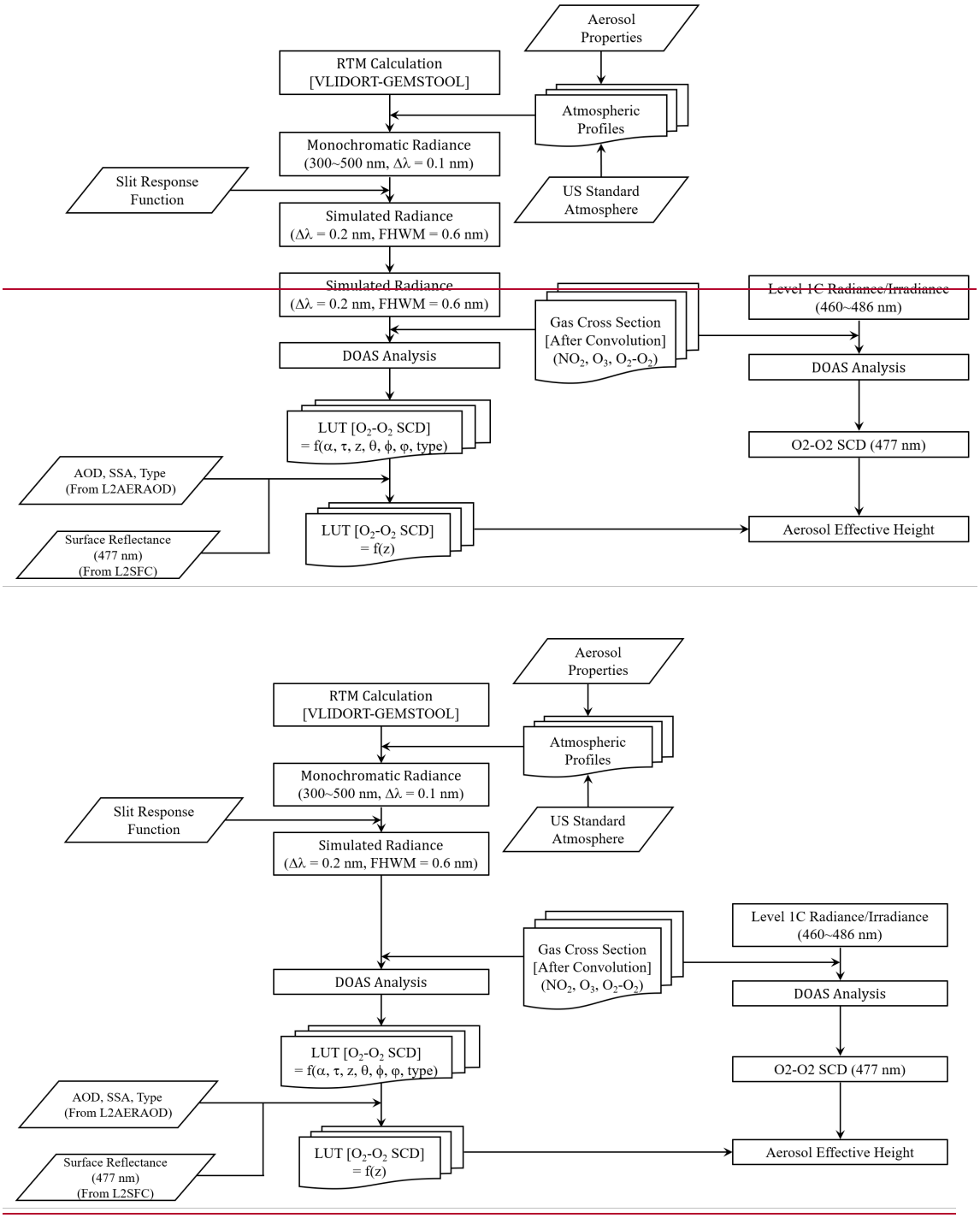

Figure ~~1~~2. Flowchart of the AEH retrieval algorithm for GEMS satellite observation.

Figure ~~1~~2 shows the overall flowchart of the AEH algorithm for GEMS satellite. The GEMS is onboard the Geostationary Korea multipurpose satellite 2B (GK2B) as

orbiting at 128.2°E, and scans from 145°E to 75°E with north-south coverage of 5°S~45°N. The GK2B observation schedule shares the GEMS and the Geostationary Ocean Color Imager 2 (GOCI2). For this reason, the GEMS scan the 30 minutes duration from every hour from 45 minutes to 15 minutes during daytime. The standard spatial resolution of GEMS is 7 × 8 km. The spectral resolution and sampling are respectively 0.6 nm with full-width and half-maximum (FWHM) and 0.2 nm with spectral range of 300~500 nm. Because the spectral coverage is limited to 300-500 nm, the AEH from GEMS is applied to the O_2-O_2 absorption band. In AEH estimation, other aerosol characteristics, including aerosol amounts and optical properties, affect retrieval accuracy.

~~The main purpose of GEMS is to monitor air quality, and aerosol properties are targets of such monitoring over East Asia. For this reason, the GEMS aerosol algorithm was developed as multiple operational products.~~ The GEMS Level 2 aerosol operational algorithm (L2AERAOD) retrieves the aerosol index (AI) values for UV and visible wavelengths, as well as AOD and SSA with considering the aerosol types (National Institute of Environmental Research, 2020a). The aerosol types are defined as absorbing, non-absorbing, and dust types by using the classification methods based on the UV and visible AIs (e.g., Go et al., 2020). Park *et al.* (2016) noted that the error budget of AEH is significantly affected by uncertainty in AOD and SSA and by the misclassification of aerosol types, which is directly related to the optical property and size information. Main error sources for AEH retrieval can be obtained from the L2AERAOD results. Therefore, the L2AERAOD results for AOD and SSA at 550 nm were adopted as input data for aerosol properties.

Although L2AERAOD retrieved their own surface reflectance for accurate separation

of surface signals from total reflectance at the top of the atmosphere (TOA), the standard product for surface reflectance (L2SFC) (National Institute of Environmental Research, 2020b) was also independently retrieved from ~~long-term~~ GEMS radiance/irradiance data with specific temporal periods. L2SFC is the reference product for spectral surface reflectance. ~~To consider the various retrieval products, the~~The L2SFC retrieves the surface reflectivity in multiple spectral channels, and retrieves the black surface reflectivity (BSR) and bi-directional reflectance distribution function (BRDF) based on the original pixel resolution. ~~Because observation geometries are limited by the geostationary satellite position, surface properties related to the directional dependency have significant uncertainty. However, L2SFC accurately retrieved surface optical properties with high spatial resolution. For this reason,~~ L2SFC was used as reference data for the surface products for all trace gas retrieval algorithms. Similarly, the AEH retrieval algorithm also uses L2SFC as a reference surface property in operation. Specifically, the BSR value at 477 nm is used as the surface reflectance input for AEH retrieval.

Table 1. Details of fitting parameter for O_2-O_2 SCD estimation via the DOAS method.

Parameter	
Fitting window	460 – 486 nm
Absorption cross section	NO_2 at 220 and 294 K (Vandaele *et al.*, 1998) O_3 at 223, 243 and 293K (Bogumil *et al.*, 2001) O_2-O_2 at 293 K (Thalman and Volkamer, 2013) Ring

For AEH retrieval, the basic method is the identification of changes in optical path length caused by effective aerosol layer height variation. To measure the optical path

length change, O_2-O_2 slant column density (SCD) retrieved by the differential optical absorption spectroscopy (DOAS) method was used. ~~From Nanda *et al.* (2020), TROPOMI uses the O_2-A band for aerosol layer height (ALH) retrieval.~~ In the GEMS product, ~~however,~~ the O_2-O_2 SCD at 477 nm absorption band is ~~used~~ most useful absorption band because this absorption band is strongest absorption band within the GEMS spectral observation range. Detailed DOAS fitting parameter and setting information is provided in Table 1 for the estimation of O_2-O_2 SCD from both the simulation and observation data. For the O2-O2 SCD estimation at 477 nm, the fitting window is ranged from 460 to 486 nm to cover the full absorption structure of O2-O2. Within the fitting window, the absorption is significantly affected by the absorptions of NO2 and O3. To describe these two absorption materials, temperature dependent cross section information are adopted. The temperature dependent cross section setting considers the stratosphere and troposphere, simultaneously. ~~After the estimation of O_2-O_2 SCD, conversion from O_2-O_2 SCD to AEH is an essential process. For this conversion, a look-up table (LUT) approach between O_2-O_2 SCD and AEH was used with consideration of observation geometries, surface conditions, and aerosol optical properties.~~

Table 2. Ratio between SCD error and the SCD of O_2-O_2 according to the polynomial order and offset settings used for DOAS fitting.

Polynomial	Offset = none	Offset = 0^{th}
2^{nd} order	6.06 ± 2.07	6.79 ± 2.31

3rd order	6.32 ± 2.20	6.79 ± 2.32
4th order	7.86 ± 2.78	7.34 ± 2.85

~~Observed radiance fitting is affected by noise signals during radiance observation.~~ To minimize the noise effect and improve fitting quality, the optimal settings for fitting were also analyzed. Table 2 shows ratios of SCD error to the SCD for various polynomial and bias orders from observed radiance. The polynomial and offset are basic fitting parameters for the DOAS fitting. Both two parameters describe the broadband spectral feature of radiance. The ratio between SCD error and the SCD of O2-O2 is important to determine the AEH retrieval quality. When the fitting error increase, the uncertainty of AEH is also enhanced during the retrieval. Although the fitting quality was good overall, the setting with 2nd order of polynomial and none offset was used for the O2-O2 SCD estimation from the GEMS radiance due to the smallest fitting error. ~~was used in this study.~~

After the estimation of O_2-O_2 SCD, conversion from O_2-O_2 SCD to AEH is an essential process. For this conversion, a look-up table (LUT) approach between O_2-O_2 SCD and AEH was used with consideration of observation geometries, surface conditions, and aerosol optical properties. Table 3 shows the dimension of the LUT for the AEH retrieval algorithm. To calculate the LUT, a linearized pseudo-spherical vector discrete ordinate radiative transfer model (VLIDORT) version 2.6 was used (Spurr, 2013). During the radiative transfer model simulation, the SSA and AOD is assumed to be 440 nm. Although the center of O2-O2 absorption is 477 nm, the spectral discrepancy between model assumed wavelength and center wavelength of O2-O2

absorption is assumed to be ignored in this study. After calculating spectral radiance with 0.1 nm sampling, we performed the slit response function of GEMS and sampling specification prior to the DOAS fitting. For O_2-O_2 absorption, the absorption cross section used for the radiative transfer model calculation is considered the temperature dependent absorption cross section (e.g., Park *et al.*, 2017). ~~The O_2-O_2 SCD error is significantly reduced with the use of simulated radiance because the simulated radiance is not considered to contain noise. By contrast, the observed radiance has a signal to noise ratio (SNR) of approximately 1000. Therefore, the observed radiance has greater fitting error than the those from the simulated radiance, although the bias between observation and simulation results is not significant.~~

O_2-O_2 SCD decreases with increasing AEH for all aerosol types and AOD (Park *et al.*, 2016). ~~In addition, the~~The O_2-O_2 SCD sensitivity is enhanced at high AOD and absorbing dominant aerosol cases. ~~Radiation is mostly scattered from the top of the aerosol layer for thick aerosols, and the effective scattering layer penetrates more deeply into the layer when the aerosol layer is thinner.~~ In addition, the contrast of O_2-O_2 SCD is greater for absorbing dominant aerosols than ~~scattering dominant aerosols~~non-absorbing aerosols. During the radiance passing through the aerosol layer, the absorbing dominant aerosol is more efficiently absorbed the radiance. For this reason, the effective optical path length is significantly shorter ~~because the optical reflection change per unit of layer depth change is large~~ for absorbing aerosols. Based on the changes in sensitivity observed for optical path length, aerosol type (in particular in terms of SSA) and AOD are considered ~~to significantly affect~~as input parameters for AEH retrieval.

Table 3. The dimension of the LUT for the GEMS AEH retrieval algorithm used to estimate AEH from O_2-O_2 SCD. (SZA: solar zenith angle, VZA: viewing zenith angle,

RAA: relative azimuth angle, SUR: surface reflectance).

Variable [unit]	No. of entries	Entries	
Spectral range [nm]	-	455~491 nm (0.1 nm interval)	
SZA [°]	7	0.01, 10, 20, 30, 40, 50, 60	
VZA [°]	7	0.01, 10, 20, 30, 40, 50, 60	
RAA [°]	10	0.01,20, 40, 60, 80, 100, 120, 140, 160, 180	
SUR	3	0.0, 0.05, 0.2	
AOD at 440 nm	9	0.04, 0.2, 0.5, 1.0, 1.5, 2.0, 2.5, 3.0, 5.0	
Refractive Index (Imaginary) at 440 nm	3×3	Absorbing (Real: 1.45)	0.000, 0.0074, 0.0314
		Dust (Real: 1.53)	0.0, 0.0030, 0.0080
		Non-Absorbing (Real: 1.41)	0.0, 0.0040, 0.0156
AEH [km]	12	0.0 (Extrapolate), 0.2, 0.5, 1.0, 1.5, 2.0, 2.5, 3.0, 3.5, 4.0, 5.0, 10.0 (Extrapolate)	
Terrain Height [km]	2	0.0, 2.0	

~~Variable [unit]~~	~~No. of entries~~	~~Entries~~
~~Spectral range [nm]~~	~~-~~	~~455~491 nm (0.1 nm interval)~~
~~SZA [°]~~	~~8~~	~~0.01,10, 20, 30, 40, 50, 60, 70~~
~~VZA [°]~~	~~8~~	~~0.01, 10, 20, 30, 40, 50, 60, 70~~
~~RAA [°]~~	~~10~~	~~0.01,20, 40, 60, 80, 100, 120, 140, 160, 180~~
~~SUR~~	~~7~~	~~0.0, 0.02, 0.05, 0.1, 0.2, 0.3, 0.5~~
~~AOD at 440 nm~~	~~9~~	~~0.04, 0.2, 0.5, 1.0, 1.5, 2.0, 2.5, 3.0, 5.0~~

~~Refractive Index (Imaginary) at 440 nm~~	~~3×7~~	~~Absorbing~~	~~0.0, 0.00206, 0.00453, 0.00738, 0.01233, 0.018, 0.02436, 0.03136~~
		~~Dust~~	~~0.0, 0.00053, 0.00113, 0.00181, 0.00298, 0.00437, 0.00603, 0.00804~~
		~~Non-Absorbing~~	~~0.0, 0.00124, 0.00258, 0.00399, 0.00547, 0.0086, 0.01197, 0.01555~~
~~AEH [km]~~	~~10~~	~~0.2, 0.5, 1.0, 1.5, 2.0, 2.5, 3.0, 3.5, 4.0, 5.0~~	
~~Terrain Height [km]~~	~~2~~	~~0.0, 2.0~~	

3. Data

3.1. TROPOMI

The TROPOMI is a spectrometer to observe the radiance from UV to near IR onboard the Sentinel-5 Precursor (Sentinel-5P) satellite. The orbit for Sentinel-5P is a polar orbit with ascending node crossing ~~to~~ the equator at 13:30 local time. The aerosol layer height product from TROPOMI (AER_LH) retrieves vertically localized aerosol layers in free troposphere with cloud free condition by using the level 1b earth radiance measurements from 758 to 770 nm (de Graaf *et al.*, 2022). The definition of ALH from TROPOMI is the optical centroid layer height of the plume. Spectral fit estimation of reflectance around the O_2-A band is based on a neural network for the forward model calculation for simulated condition. After cloud masking to avoid the cloud affected pixels, an optimal estimation method was used to retrieve the aerosol layer height parameters for the inversion method from observation. During the radiance fitting, the ALH and AOD are fitted parameters ~~is also used as the main fitting parameter~~, but other aerosol parameters, such as SSA, layer thickness, and scattering phase function, are assumed to be fixed values (Nanda et al., 2020). The target requirement on the accuracy

and precision is 0.5 km or 50 hPa, and the threshold requirement is 1 km or 100 hPa (de Graaf et al., 2022). In this study, we use version 2.0.0 of the TROPOMI offline level 2 AER_LH product with the spatial resolution is 3.5 km × 7 km at nadir viewing geometry.

3.2. CALIOP

The CALIOP is a spaceborne lidar ~~sensor~~ onboard the Cloud-Aerosol Lidar and Infrared Pathfinder Satellite Observations (CALIPSO) to measure the vertical information of aerosol and cloud with estimating the optical properties. The CALIOP has two different wavelength channels (532 and 1064 nm) by using the Nd:YAG laser to generate the signals (Winker et al., 2009). ~~This sensor~~The orbit for CALIPSO is Sun synchronous orbit constellated to the A-train with ascending node, and also crosses to the equator at 13:30 local time ~~by ascending node~~. For the vertical information, the resolution for vertical sampling is 30 m below 8 km altitude, and 60 m from 8 to 20 km altitude, respectively. Although the pixel data can retrieve with extremely high horizontal and vertical resolutions, the spatial coverage is narrow. In this study, the data of Level 2 aerosol profile product (APro, version 3.41) was used. ~~Because the aerosol profile product exists the vertical distribution of aerosol extinction coefficient,~~ ~~r~~Representative layer height parameters (ALH and AEH) ~~is~~ are directly estimated by using the vertical profile of aerosol extinction coefficient at 532 nm.

4. Case studies

Figure ~~2~~ 3 shows retrieval results for AEH, AOD, and SSA from GEMS on March 29 over East Asia. Because the operational schedule is hourly during the daytime, the

GEMS retrieval results are shown at 1-hour intervals from 01:00 to 07:00 Universal Time Coordinated (UTC). ~~Based on the retrieval sensitivity of AEH~~From Park et al. (2016), thin AOD pixels have large AEH uncertainty due to weak aerosol scattering information. For this reason, only AEH retrieval results with AOD greater than 0.3 are shown in this study. During this case study, a Yellow dust plume was located along the coast of China and South Korea with AOD at 443 nm of 0.8~1.2. Simultaneously, another plume was also present over the northeastern Korean Peninsula with AOD of 1.0~2.0 at 443 nm. SSA at 443 nm was 0.90~0.93 for the plume over South Korea and 0.87~0.90 for the plume over the northeastern Korean Peninsula. Although the AOD and SSA for these plumes are differed significantly, ~~their~~ the retrieved AEH results from these different plumes show similar ranges~~were similar~~. For both plumes, AEH shows around 1.0~2.0 km in this case. ~~In addition, the retrieved AEH values exhibited insignificant diurnal variation in regions with severe dust plumes.~~

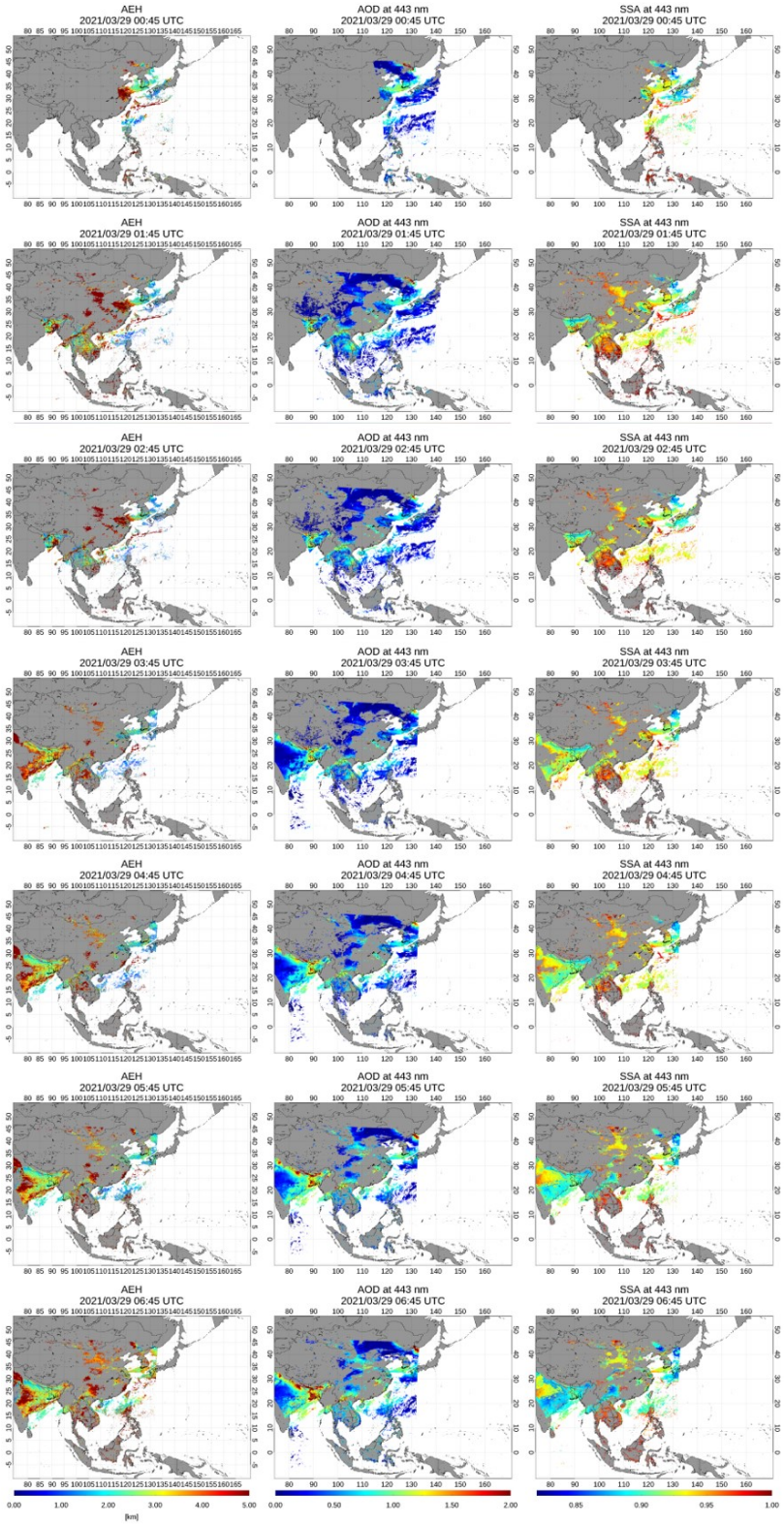

Figure ~~2~~3. Case study results for AEH, AOD, and SSA based on GEMS observations on March 29, 2021.

As shown in Figure ~~2~~3, an additional severe aerosol plume was present over northeastern India, with AOD at 443 nm of 1.0~2.0 and SSA at 443 nm of 0.85~0.90. From Rana *et al.* (2019), metropolitan cities and industrial cluster in India are heavy emitters of black carbon, and high concentrations of black carbon are distributed over the Indo-Gangetic Plain (IGP). Therefore, the aerosol plume with high AOD and low SSA (high absorbing) was ~~significant~~a result that actually exists, and it was not a result with high uncertainty due to edge of GEMS observation field. Except for the inland parts of India, AEH in ~~severe aerosol plumes~~high AOD pixels ranged from 1.5 to 3.5 km.~~, and AEH was stably estimated across the entire observation period.~~

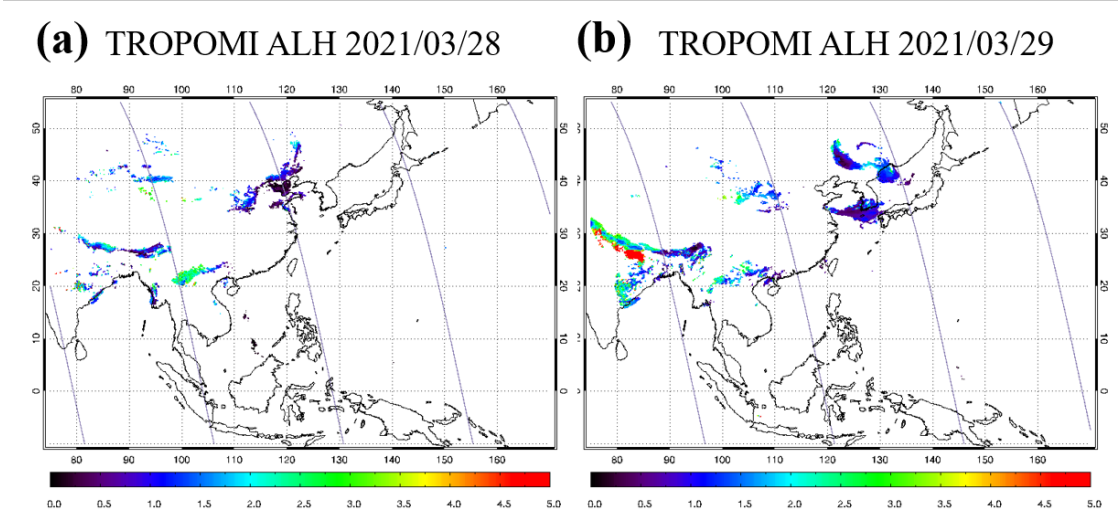

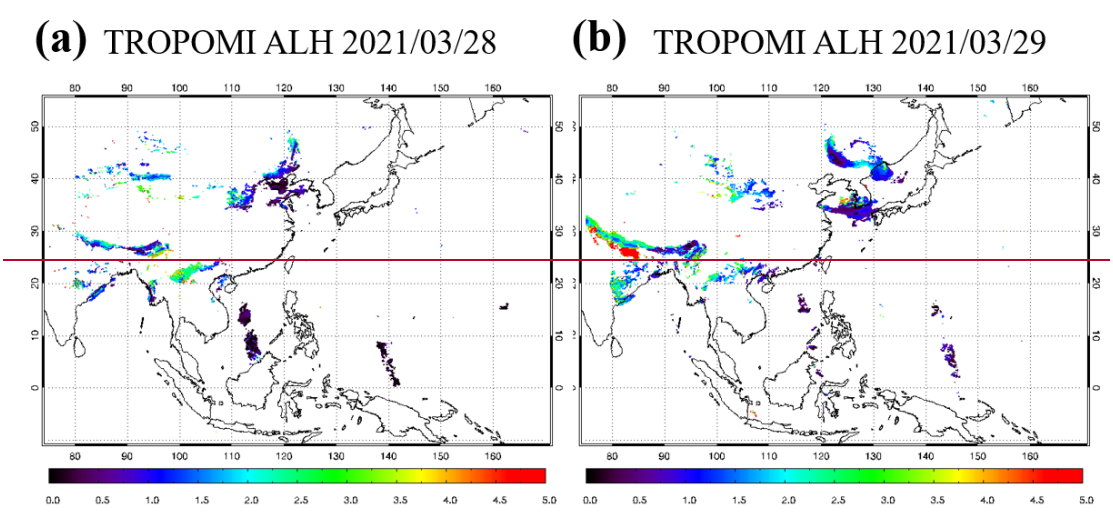

Figure 4. ALH retrieved from TROPOMI and orbit path of CALIOP on (a) March 28 and (b) March 29, 2021 (Unit: km).

~~**Figure 3.** ALH retrieved from TROPOMI on (a) March 28 and (b) March 29, 2021.~~

For comparison of the retrieval, Figure ~~3~~ 4 shows the ALH retrieved from TROPOMI on March 28 and 29, 2021 over East Asia. A dust plume was transported from China to South Korea during this period, then split into two distinct plumes over northeastern China and the coastal area of South Korea. The ALH retrieved from TROPOMI for both plumes were 0.5~1.5 km. ~~The definition of ALH from TROPOMI is the optical centroid layer height of the plume. Otherwise, the AEH product from GEMS is defined as the height with aerosol extinction integrated from the surface of $(1-\exp^{-1})$ × AOD.~~ Given ~~this~~ the difference in definition for the aerosol height parameters between ALH and AEH, ~~larger aerosol heights~~relatively high height values were retrieved from GEMS compared to TROPOMI. In an ideal case under symmetric gaussian distribution with a width of 1 km, the AEH from GEMS was around 0.5 km higher than the peak height of aerosol layer. The ALH expresses the center (or peak) height, thus, the AEH from GEMS was overestimated by around 0.5 km relative to the ALH from TROPOMI.~~,~~ ~~assuming the aerosol vertical distribution was a Gaussian with a width of 1 km.~~ Although AEH had higher values than ALH from TROPOMI, the GEMS AEH retrievals for the dust transport case study were ~~good~~successfully retrieved and mostly shown the expected uncertainty of 1 km.

Furthermore, the ~~retrieval area~~AEH retrieved pixels covered by GEMS is larger than by TROPOMI, as demonstrated by a comparison of Figures ~~2~~ 3 and ~~3~~4. In East Asia, AEH from GEMS estimated a continuous dust plume from China to South Korea. In

addition, the GEMS retrieval ~~results~~more widely estimated ~~greater~~ aerosol height information in coastal India compared to TROPOMI. Although high AEH values were retrieved for low AOD regions over low latitude ocean surface, ~~high height values were retrieved for clear-sky regions, in particular low latitude ocean regions,~~ the AEH from GEMS was successfully retrieved over the area of interest for the case study.

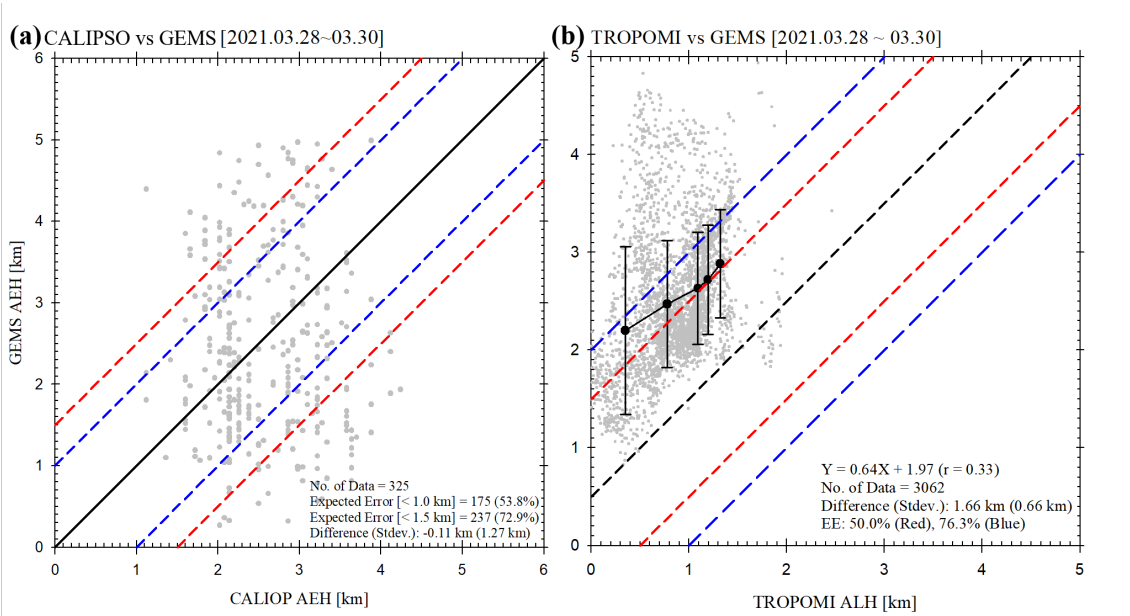

Figure 5. Intercomparison of (a) AEH between CALIOP and GEMS and (b) ALH from TROPOMI and AEH from GEMS (black dot and error bar is mean and standard deviation in 20% interval of each TROPOMI ALH) over the period from March 28 to 30, 2021.

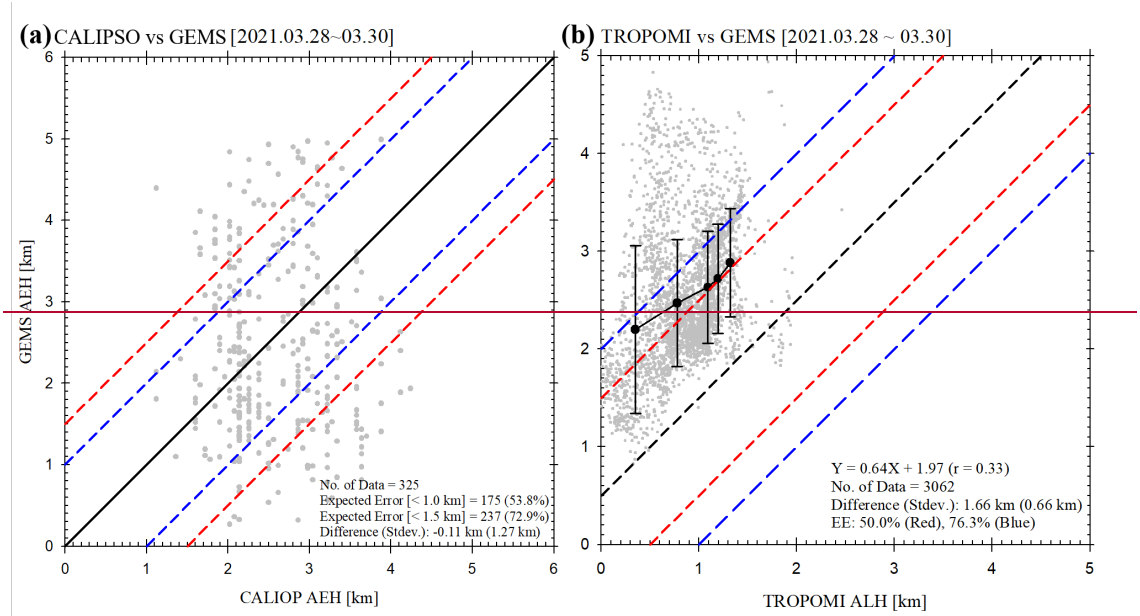

~~**Figure 4.** Intercomparison of (a) AEH between CALIOP and GEMS and (b) ALH~~

~~from TROPOMI and AEH from GEMS over the period from March 28 to 30, 2021.~~

Figure ~~4~~ 5 shows intercomparison results for aerosol plume height among GEMS, CALIOP, and TROPOMI during the case study of Yellow dust transport in East Asia from March 28 to 30, 2021. For spatial colocation, we selected pixels for which distance between GEMS and CALIOP observations was less than 50 km. In addition, only the closest 10% of pixels were used. Given the different orbital characteristics of CALIOP and GEMS, temporal colocation was also considered. During the period of image scanning from east to west over Asia by GEMS, CALIOP passes through the GEMS observation area from south to north every 98.3 minutes. On average, CALIOP passes three to four orbits through the GEMS scan area during a single day of daytime observation. To consider these different orbital characteristics, temporal colocation was limited to a 1-hour difference between CALIOP and GEMS scans. As GEMS observes hourly, colocated pixels between the two satellites shift from east to west over time. Ultimately, the number of colocated pixels with AOD at 443 nm > 0.3 was 534 for this case study.

For the direct comparison shown in Figure ~~4a~~5a, the difference in AEH between GEMS and CALIOP was -0.11±1.27 km. Nanda *et al.* (2020) reported that the difference in ALH between TROPOMI and CALIOP was 0.53 km for 4 cases of thick Saharan dust plumes. In addition, 53.8% and 72.9% of the total pixels showed differences less than 1.0 and 1.5 km, respectively. Large AEH uncertainty occurred mostly over the inland area of China. Because AEH from GEMS uses only the O_2-O_2 absorption band, the accuracy of AEH is sensitive to uncertainty in surface reflectance and AOD. ~~Although~~ Recently, GEMS accurately estimated surface reflectance in near

real time in operation~~,~~. However, this study used the minimum reflectance under the Lambertian assumption to retrieve AOD and AEH to coincide with the use of surface information on L2AERAOD and AEH retrieval~~. For this reason, the retrieved results were significantly affected by uncertainty in surface properties during the observation period.~~

Figure ~~4b~~ 5b shows a comparison of GEMS and TROPOMI for the period of March 28 ~ 30, 2021 in East Asia. To ensure the accuracy of ALH from TROPOMI, only pixels with quality assurance (QA) values greater than 0.5 were used. The difference between GEMS AEH and TROPOMI ALH was 1.66 ± 0.66 km in this case, and 49.9% of all pixels had differences less than 1.5 km. This proportion value was lower than the corresponding result from the comparison of GEMS and CALIOP. However, the ALH from TROPOMI is generally lower than the AEH from GEMS because of the discrepancy in definitions. To correct the inconsistency of definition between ALH and AEH, the difference between two retrieval results decreased to 0.5 km bias. After correction, 50.0% and 76.3% of pixels are within the expected error ranges of 1.0 and 1.5 km, respectively.

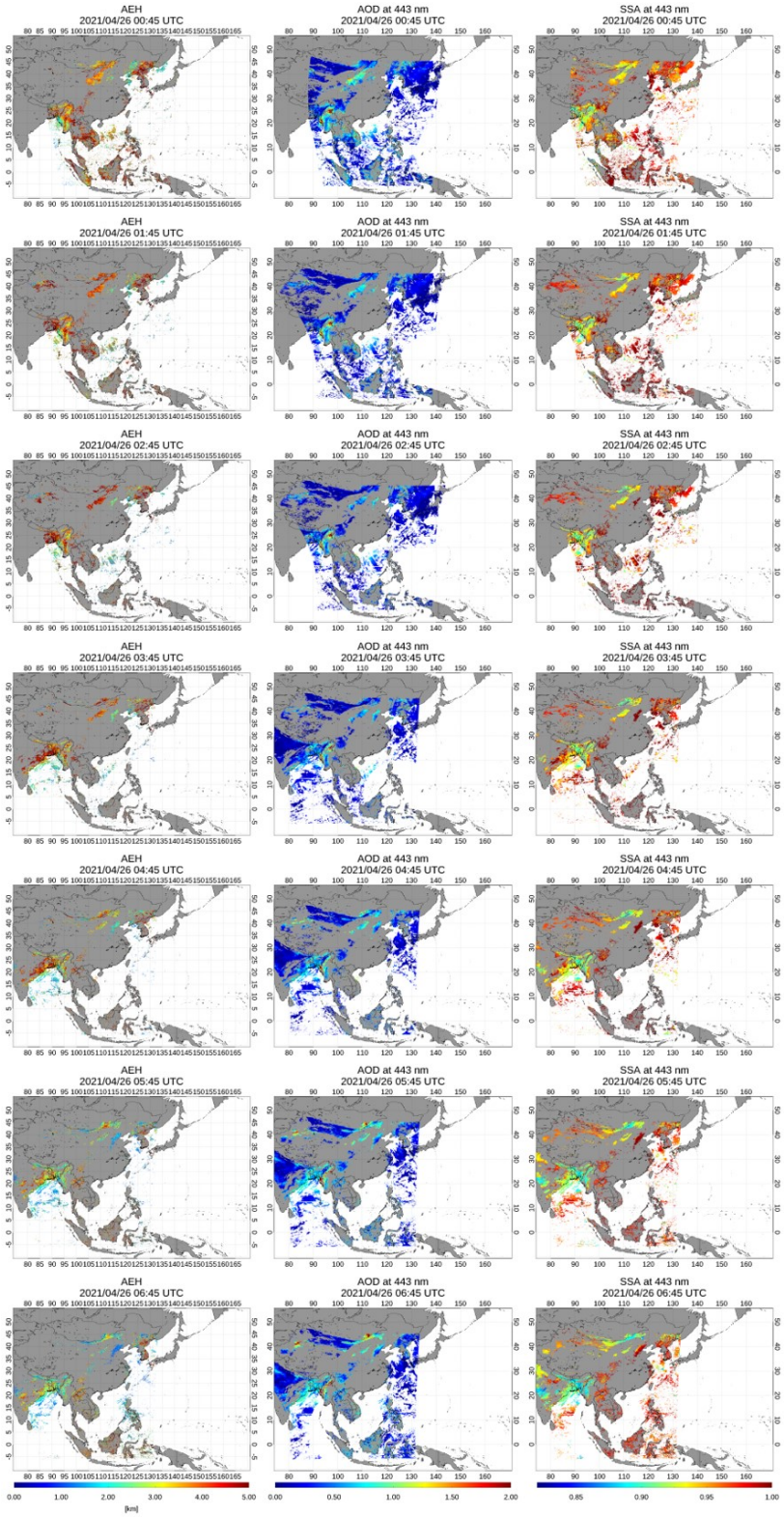

438

439 **Figure 56.** Case study results for AEH, AOD, and SSA based on GEMS observations

440 on April 26, 2021.

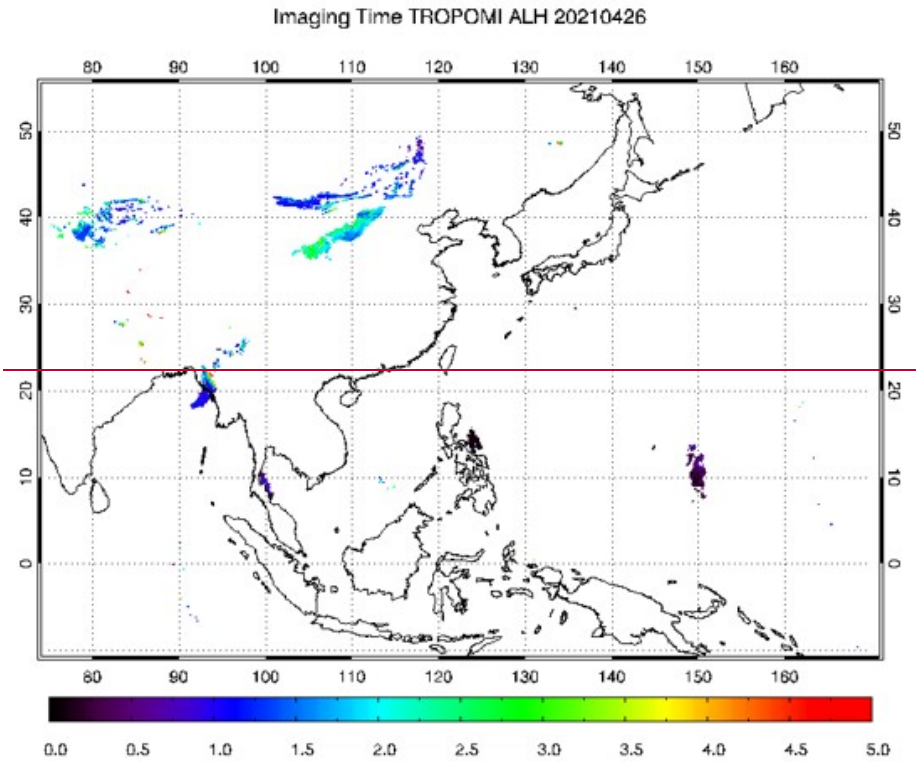
Imaging Time TROPOMI ALH 20210426
80
90
100
110
120
130
140
150
160
0
10
20
30
40
50
0.0
0.5
1.0
1.5
2.0
2.5
3.0
3.5
4.0
4.5
5.0

441

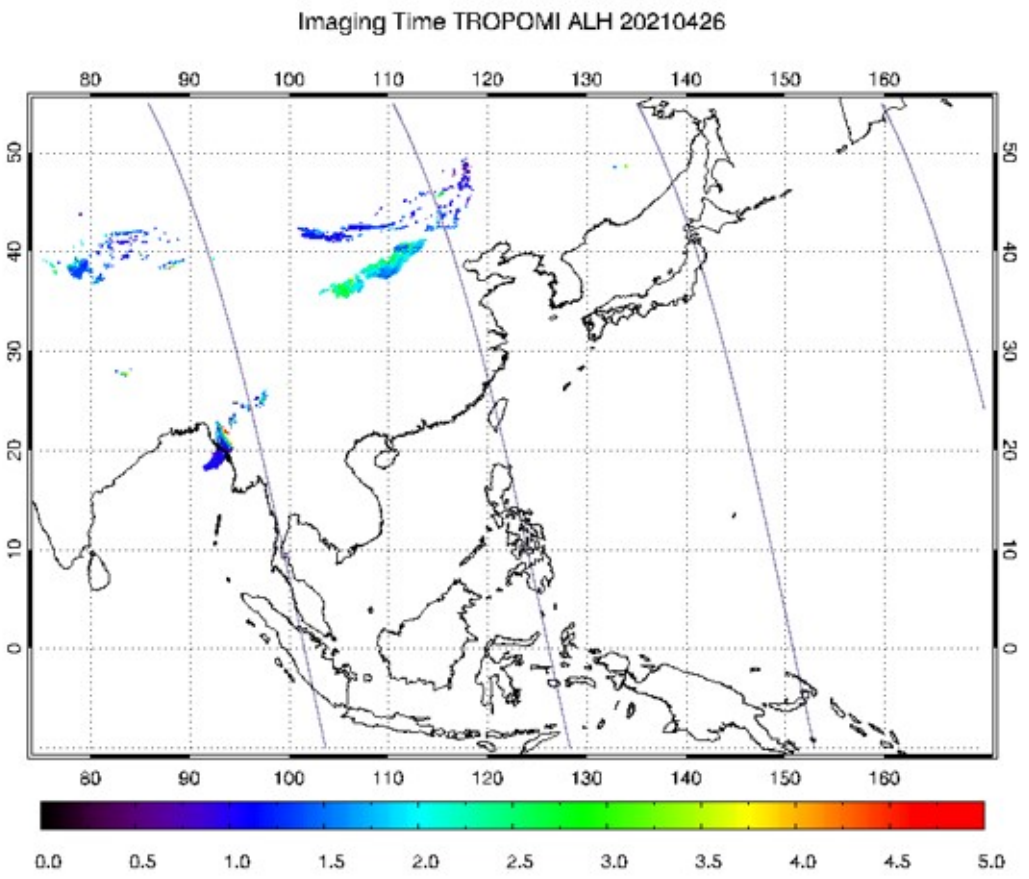

Figure 76. ALH retrieved from TROPOMI and orbit path of CALIOP on April 26, 2021 (Unit: km).

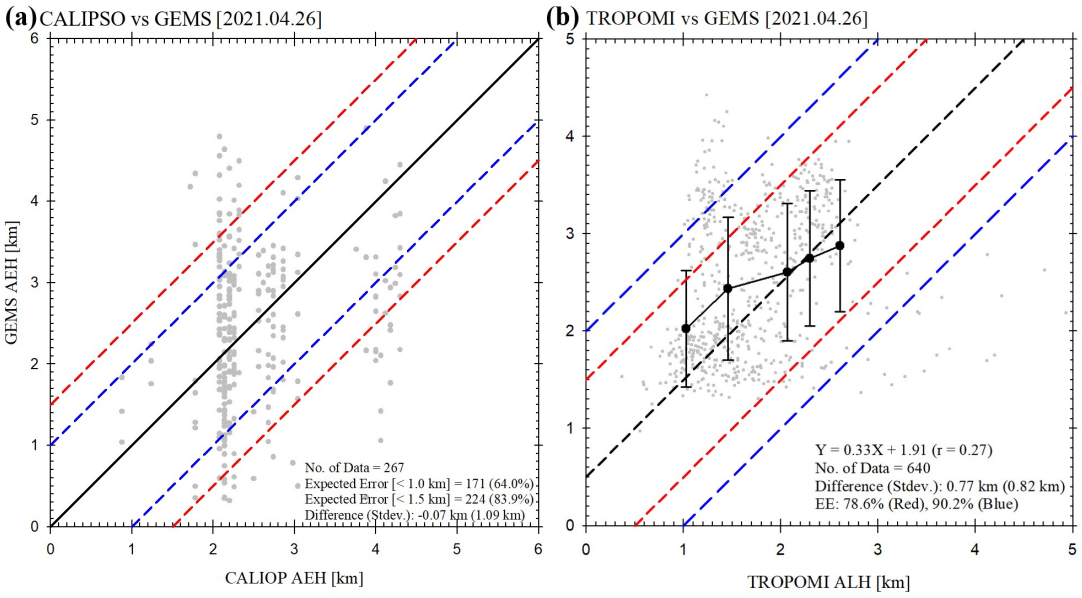

Figure 8. Intercomparison of (a) AEH between CALIOP and GEMS, and (b) ALH from TROPOMI and AEH from GEMS (black dot and error bar is mean and standard deviation in 20% interval of each TROPOMI ALH) on April 26, 2021.

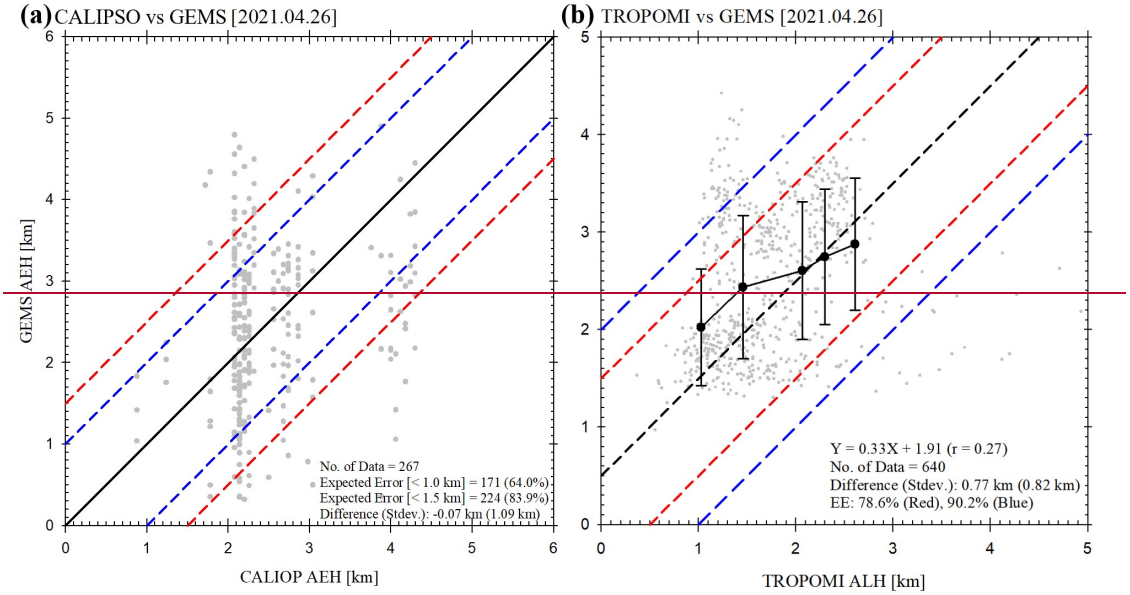

~~**Figure 7.** Intercomparison of (a) AEH between CALIOP and GEMS, and (b) ALH from TROPOMI and AEH from GEMS on April 26, 2021.~~

An additional intercomparison case of April 26, 2021 is shown in Figures ~~5~~–6 (GEMS) and 7~~6~~ (TROPOMI). During the transport of the Yellow dust plume from inland China to the coastal area, AEH changed from 4.0 km at 02:00 UTC to 2.0 km at 06:00 UTC. By contrast, ALH from TROPOMI only observed the 1.5~2.5 km layer height over East Asia around 04:00 UTC. Although the AEH from GEMS had spatio-temporal uncertainty, this case demonstrates the advantage of AEH retrieval from GEMS for continuous monitoring of changes in plume height, in particular during dust transport. As shown in Figure ~~7~~8, AEH from GEMS showed differences in height of -0.07 ± 1.09 km (compared to CALIOP) and 0.77 ± 0.82 km (compared to TROPOMI).

~~These comparison results show that the GEMS algorithm accurately retrieved AEH and can be used in several application studies.~~

5. Long-term validation

For long-term validation, we used the AEH retrieval results from January to June, 2021. Similar to the case studies, intercomparison datasets from CALIOP and TROPOMI were selected containing mean layer height values in the closest 10% of pixels within a 50 km range for spatial colocation. In addition, only observations taken within ±1 hour of the GEMS observation time were selected for temporal colocation. As the CALIOP and TROPOMI satellites passed over the study area around 13:30 local time, which is around 04:30 UTC for East Asia and around 06:30 UTC for India. Most temporal colocation pixels aligned with observation times of 04:00~06:00 UTC, respectively. To check the dependence of several retrieval variables, the AI value for UV (UVAI), AOD, SSA, and dominant aerosol type in each pixel (TYPE) were obtained from the L2AERAOD. Although the GEMS algorithm retrieved AEH in the range of 0~10 km, the sensitivity of O_2-O_2 SCD was weak in cases of high AEH because of the vertical distribution of air molecules. To ensure sufficient quality of retrieved data, therefore, the AEHs from GEMS and CALIOP, and the ALH from TROPOMI were used only in pixels where the AEH from GEMS were lower than 5 km.

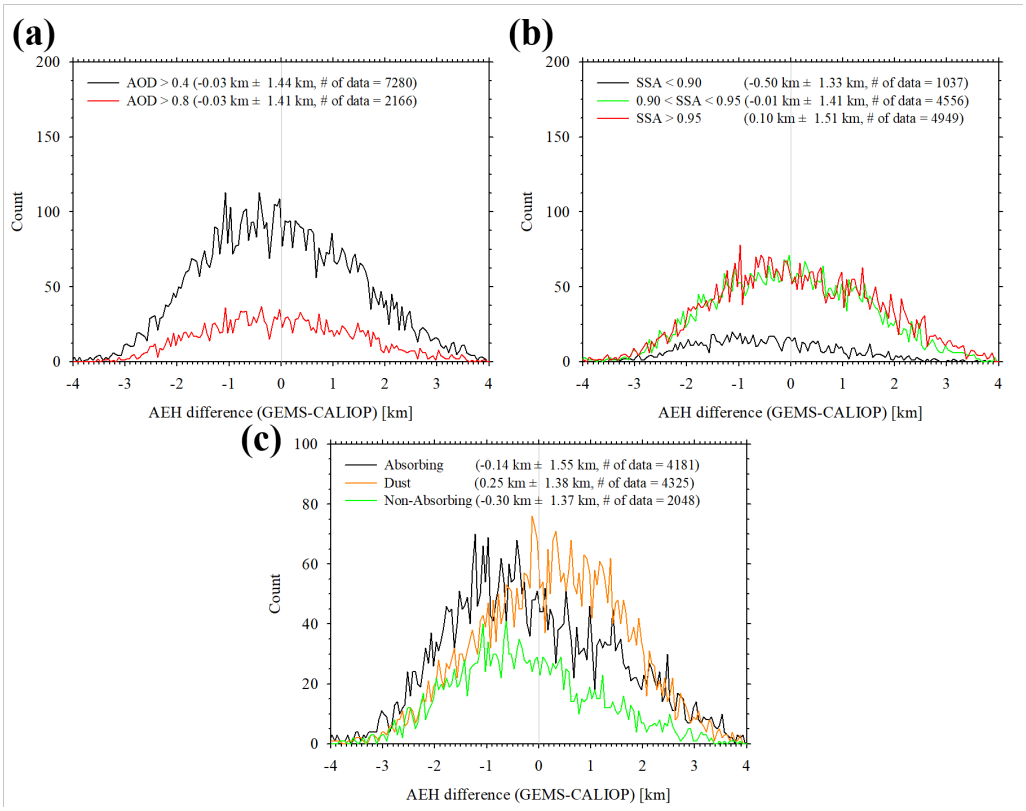

Figure 98. Histogram of AEH difference between CALIOP and GEMS with respect to (a) AOD, (b) SSA, and (c) TYPE from GEMS over the period from January 1 to June 30, 2021.

Figure 8 9 shows histograms of difference in AEH between GEMS and CALIOP according to AOD at 443 nm, SSA at 443 nm, and TYPE from GEMS. From Figure 89a, the dependence on AOD threshold was insignificant; the average estimated AEH difference was -0.03 km, but the variation in AEH difference was around 1.4 km based on the standard deviation for AOD > 0.4. Because of uncertainty in GEMS operational products, AEH from GEMS exhibits large variability. ~~As reported by Park *et al.* (2016), error budgets of AEH from O_2-O_2 SCD were 105~387, 72~352, and 576~1047 m because of uncertainty in AOD, aerosol particle size, and SSA, respectively.~~ Although

L2AERAOD from GEMS ~~accurately~~ retrieved the AOD, SSA, and aerosol types~~optical and physical properties of aerosols (AOD, SSA, and TYPE)~~, the retrieved results from L2AERAOD include significant uncertainty~~still remained significant uncertainty~~. Go *et al.* (2020) noted that the UV aerosol retrieval algorithm, which is the basic method to the L2AERAOD algorithm, has significant ~~root mean square errors (RMSEs)~~discrepancies for both AOD and SSA compared to ground-based data. In addition, significant fitting error perturbs the fitting signals and tends to result in the underestimation of SCD. Although the fitting error of O_2-O_2 SCD from GEMS radiance was minimized, the fitting error is still remained around 6%, as indicated in Table 2. The discrepancy in fitting condition between the simulated and observed radiance biased the SCD estimation, which in turn led to bias and variation in the AEH retrieval. Combined with the high sensitivity of AEH errors to aerosol optical properties, uncertainty arising from L2AERAOD causes significant variability in AEH.

~~Additional potential sources of error for AEH from GEMS are uncertainty in surface reflectance and the discrepancy in O_2-O_2 SCD values between the simulation results and observations. Park *et al.* (2016) found that O_2-O_2 SCD significantly alters the surface reflectance and is an error source affecting AEH retrieval. Although the fitting error of O_2-O_2 SCD from GEMS radiance was minimized, the fitting error is still remained around 6%, as indicated in Table 2. Significant fitting error perturbs the fitting signals and tends to result in the underestimation of SCD. The discrepancy in fitting condition between the simulated and observed radiance biased the SCD estimation, which in turn led to bias and variation in the AEH retrieval.~~

The variation in AEH difference between observation platforms is shown in Figure ~~8b~~ 9b as a histogram according to SSA threshold. Across the entire SSA threshold range,

518 the standard deviation of the AEH difference was 1.33~1.51 km. In particular, this
519 standard deviation decreased slightly with decreasing SSA. Aerosol height information
520 is significantly more sensitive to absorbing-dominant aerosols than scattering-dominant
521 aerosols (e.g., Park *et al.*, 2016; Nanda *et al.*, 2020). Even if the uncertainty due to
522 aerosol properties is fixed, the variability of AEH is affected by the sensitivity of AEH
523 error to aerosol absorptivity.

524 Figure ~~8c~~ 9c shows the dependence of AEH difference on TYPE. Changing the Type
525 significantly changed the mean value of AEH difference. The TYPE product included
526 dependence on the aerosol size and optical absorptivity. For this reason, the AEH
527 difference graphs for the "Dust" and "Absorbing" types differ, despite both types being
528 absorbing-dominant aerosols. The AEH difference for the "Absorbing" type showed a
529 negative bias with a large standard deviation, whereas a positive bias with a small
530 standard deviation was obtained for the "Dust" type. The AEH difference for the "Non-
531 Absorbing" aerosol type showed the largest negative bias in this comparison. These
532 results suggest that the aerosol size distribution of fine particles affects the negative bias
533 of AEH. Combined with the AEH difference bias illustrated in Figure 8b, these findings
534 indicate that the bias in AEH difference for "Absorbing" aerosols is weakened by their
535 absorbing-dominant property.

536 Figure ~~9~~10 shows means and standard deviations for AEH difference between
537 CALIOP and GEMS according to AOD and AI values from GEMS. For AOD, the mean
538 AEH difference ranged from -0.13 to 0.03 km with a standard deviation of
539 approximately 1.45 km. Similar to Figure ~~8a~~9a, the variation in AEH difference with
540 AOD change was insignificant. For AI, the smallest AEH difference was -0.19 km,
541 obtained for the AI range of 1.5~2.0. The largest AEH difference was 0.24 km for the AI

range of 4.0~4.5. Although the AEH difference varied slightly, no consistent tendency in AEH variation with AI was observed Overall, the standard deviation of AEH difference ranged from 1.49 km (0.0 < AI < 0.5) to 1.18 km (4.5 < AI < 5.0), and a consistent tendency of decreasing variance in AEH difference was found with increasing AI.

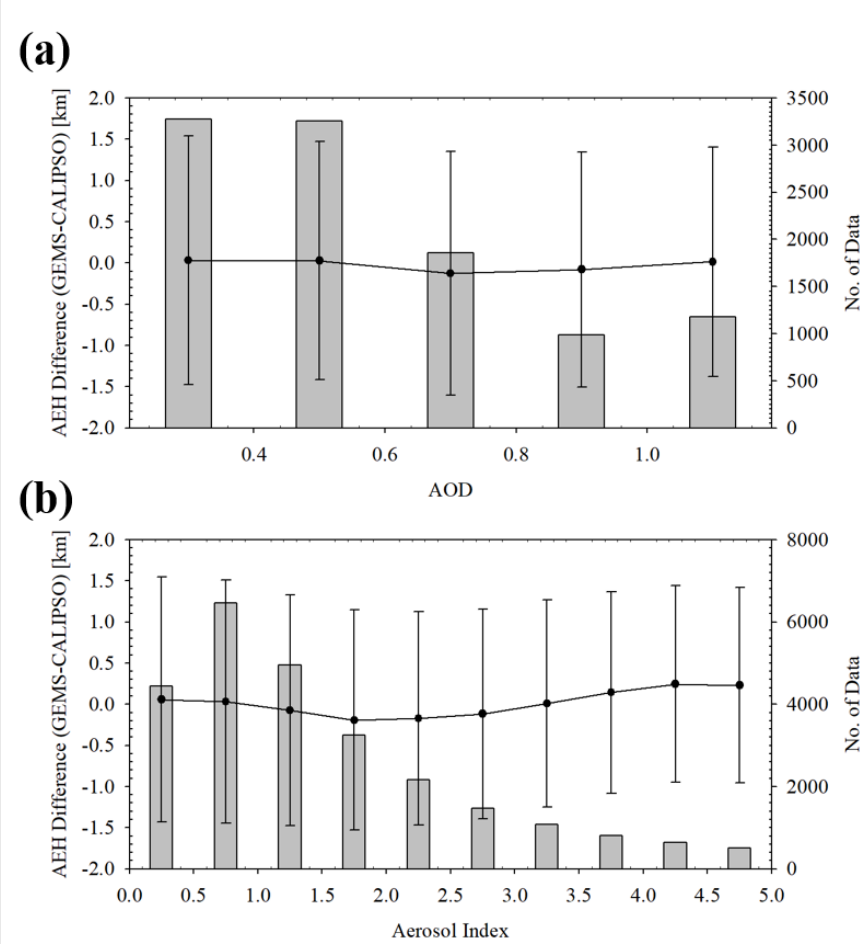

Figure ~~9~~10. AEH difference between CALIOP and GEMS with respect to ranges of (a) AOD and (b) AI obtained from GEMS from January 1 to June 30, 2021 (line and error bar is the mean and standard deviation of AEH difference, and the box is number of data).

Figure ~~10~~ 11 shows histograms of differences between ALH from TROPOMI and

AEH from GEMS [(AEH from GEMS) – (ALH from TROPOMI)] according to the SSA and TYPE obtained from GEMS. As TROPOMI retrieved only ALH data with high QA values over pixels containing strong aerosol plumes, the AOD dependence of aerosol height difference is not shown in this comparison. In addition, the number of pixels corresponding to ~~scattering dominant~~non-absorbing aerosols (i.e., pixels with SSA > 0.95 or "Non-Absorbing" type) was insufficient. Nanda *et al.* (2020) showed that the operational algorithm of TROPOMI is only retrieved the ALH over absorbing dominant aerosol pixels. ~~limited to retrieving the ALH over scattering dominant aerosols.~~ In addition, Griffin *et al.* (2020) reported that the pixels with small positive UVAI (weak absorbing cases) pixels ~~small absorbing AI pixels~~ are identified with small QA values in the offline product of ALH.

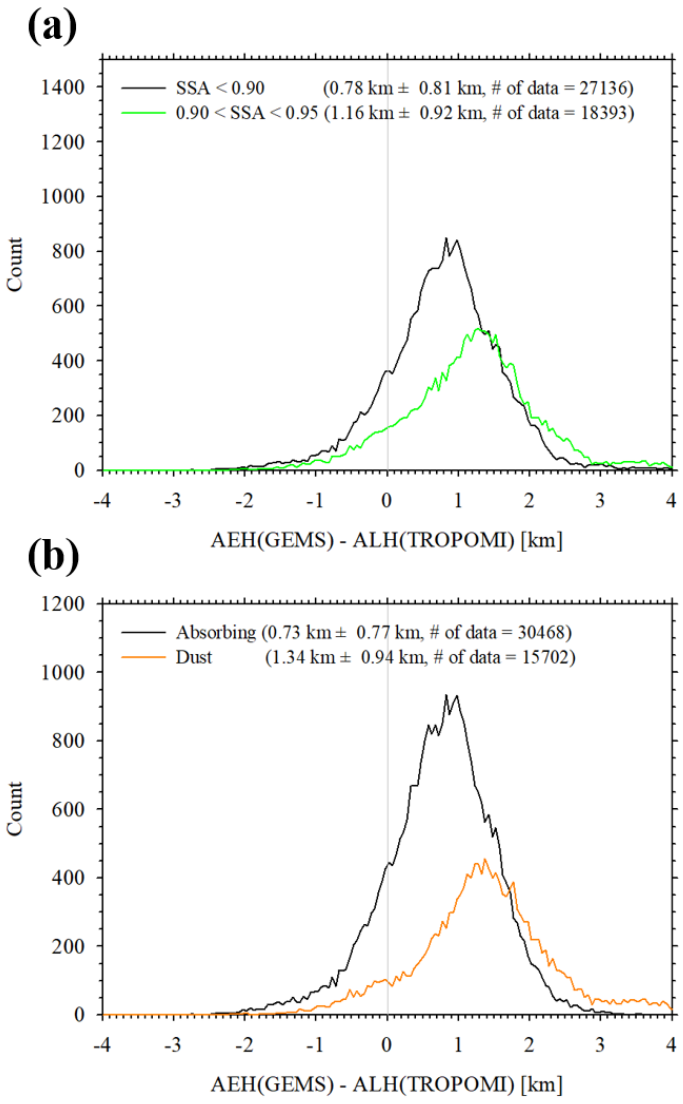

564

565 **Figure ~~10~~11.** Histograms of differences between ALH from TROPOMI and AEH
566 from GEMS [(AEH from GEMS) – (ALH from TROPOMI)] with respect to (a) SSA,
567 and (b) TYPE from GEMS in the period from January 1 to June 30, 2021.

568 As shown in Figure ~~10~~11, (AEH from GEMS) – (ALH from TROPOMI) was
569 significantly dependent on both SSA and TYPE. The mean value of (AEH from GEMS)
570 – (ALH from TROPOMI) decreased as the aerosol absorptivity increased. This
571 difference was 0.78 ± 0.81 and 1.16 ± 0.92 km for pixels of SSA < 0.90 and 0.90 < SSA
572 < 0.95, respectively. Comparing these results to Figure 8b, we find that the standard

deviation of the comparison with TROPOMI was approximately 60% of the corresponding value for CALIOP. ~~This smaller variability compared to CALIOP~~It is because ~~appears to have arisen because~~ both TROPOMI and GEMS are passive sensors that use similar retrieval methods for oxygen ~~related~~ absorption bands.

In addition, (AEH from GEMS) – (ALH from TROPOMI) was significantly dependent on TYPE, as shown in Figure 10b. The difference was 0.73 ± 0.77 and 1.34 ± 0.94 km for "Absorbing" and "Dust" type aerosols, respectively. Similar to Figure 8c, the TYPE dependence of aerosol height information was influenced by both absorptivity and size information. In addition, the difference in the definition of ALH from TROPOMI and AEH from GEMS impacted the comparison. "Dust" types of aerosol are mainly transported in the free troposphere, and the associated plume thickness is highly variable. By contrast, "Absorbing" aerosols mainly originate from anthropogenic emissions in East Asia (e.g., Gao *et al.*, 2014; Wang *et al.*, 2012; Peng *et al.*, 2016). In addition, the vertical distribution of aerosols is unstable for "Dust" case. For these reasons, the standard deviation of aerosol height was larger for the "Dust" type.

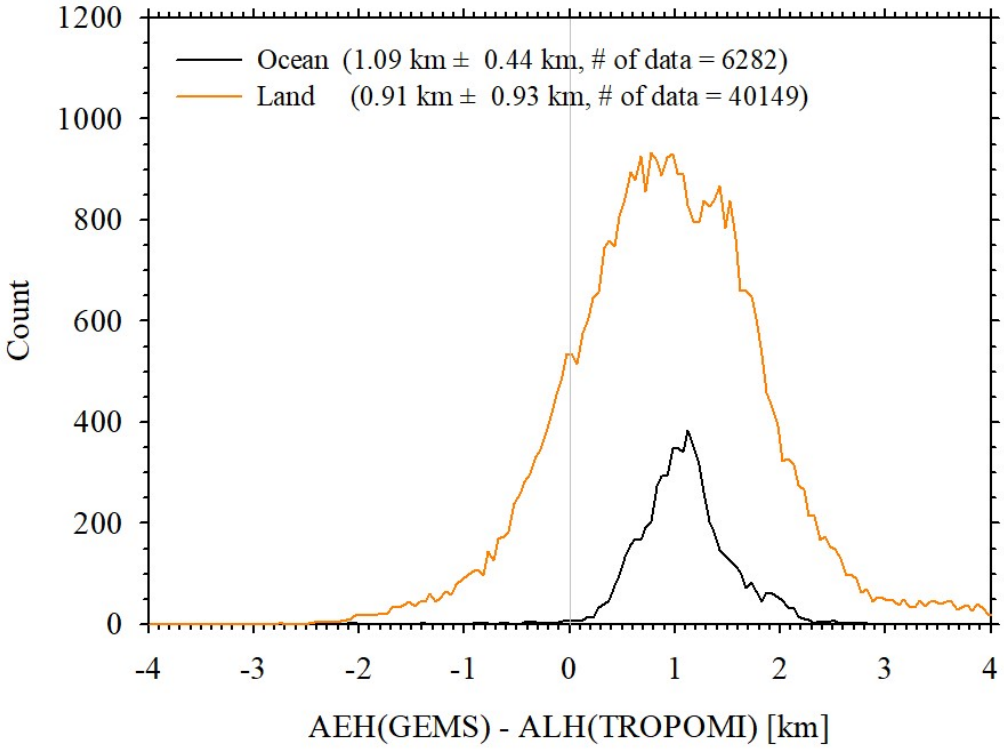

589

590 **Figure ~~11~~12.** Histogram of the difference between ALH from TROPOMI and AEH
591 from GEMS [(AEH from GEMS) – (ALH from TROPOMI)] over land and ocean pixels,
592 respectively, from January 1 to June 30, 2021.

593

594 The non-Lambertian effect on the land surface impacted surface albedo uncertainty
595 during AEH retrieval, and this effect led to bias and variance in AEH. In this study, the
596 minimum Lambertian equivalent reflectance was used as the reference reflectance value.
597 However, surface reflectivity has geometric dependence due to non-Lambertian effects,
598 which leads to a bias of 0.01-0.02 for surface reflectance over the land surface (e.g., Qin
599 *et al.*, 2019). To identify the sensitivity of surface property, a histogram was constructed
600 of (AEH from GEMS) – (ALH from TROPOMI) after classification into land and ocean
601 surface types, as shown in Figure ~~11~~12. From the statistical results, the mean differences

were estimated to be 1.09 and 0.91 km for ocean and land pixels, respectively, indicating insignificant difference in bias between these two surface covers. However, the standard deviation of the two surface types indicated a significant difference. Over the ocean surface, the histogram is very narrow. Although there are 6.5 times more data for land than those for the ocean surface, the land surface has a relatively wide histogram distribution. This discrepancy arises because the non-Lambertian effect causes bias in surface reflectance, while also influencing the variability in surface reflectance related to observation geometry. For this reason, land surface reflectance based on the non-Lambertian surface assumption is not fully representative of actual surface reflectance as a function of observation geometry. Therefore, the standard deviation of the layer height difference is larger over the land surface, and the significant difference between land and ocean pixels is mainly driven by the assumption of surface reflection properties.

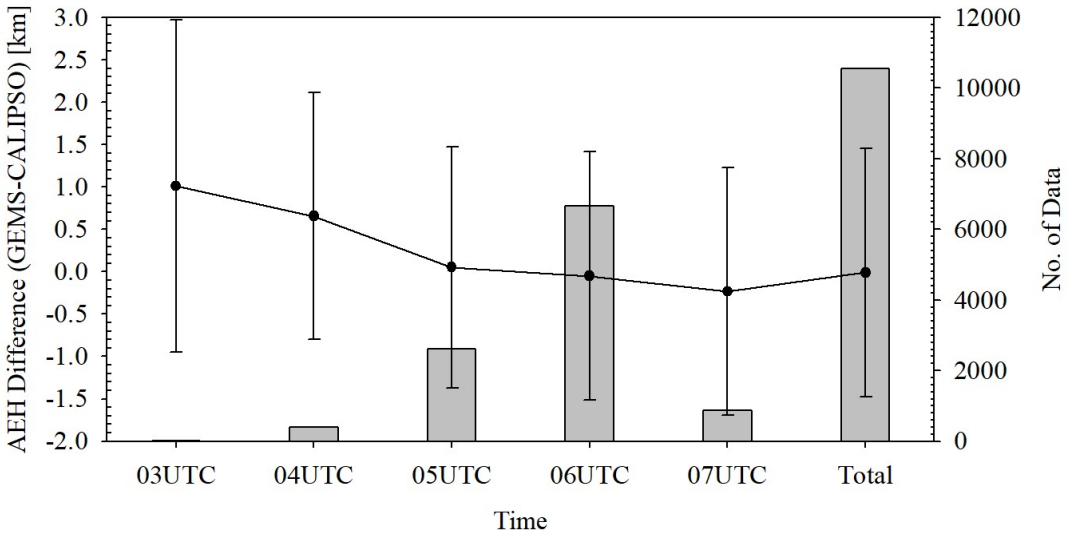

Figure ~~12~~13. Diurnal dependence of AEH difference between CALIOP and GEMS from January 1 to June 30, 2021 (line and error bar is the mean and standard deviation

of AEH difference, and the box is number of data).

The results of hourly statistical analyses are presented in Figure ~~12~~13. Because they use a consistent definition of AEH, we show only a comparison of GEMS and CALIOP. The diurnal variation in AEH difference ranged from -0.23 ± 1.45 km (07:00 UTC, Number of Data = 867) to 1.01 ± 1.96 km (03:00 UTC, Number of Data = 23). However, the number of pixels observed at 03:00 UTC was insufficient for the identification of diurnal variation. The AEH difference of 0.66 ± 1.45 km was the next highest value obtained at 04:00 UTC (Number of Data = 395). The inhomogeneous number of data is mainly due to the lack of spatial homogeneity among retrieval pixels. Over India, very high AOD values were consistently observed during the comparison period. Otherwise, the AEH was only retrieved under conditions of severe anthropogenic emissions over East Asia. In addition, the diurnal variation in AEH difference was caused by spatial characteristics of AEH difference. From 03:00 to 05:00 UTC, CALIOP mainly passed over East Asia, which has numerous sources of aerosol emissions, including biomass burning, dust, and industrial activity. In addition, GEMS observed only the eastern part of India, which is dominated by anthropogenic aerosols. The spatial distribution of the dominant aerosol types may impact the diurnal variation in AEH difference.

6. Summary & Conclusions

Based on the possibility of retrieving AEH from environmental satellite sensors, an AEH retrieval algorithm for GEMS was developed that solely uses the O_2-O_2 absorption band with considering aerosol and surface properties. Because the sensitivity of AEH

642 retrieval is strongly affected by optical amounts and properties of aerosols, as well as
643 surface reflectivity, an AEH retrieval algorithm for GEMS was developed after retrieval
644 of the GEMS operational algorithms, L2AERAOD and L2SFC. With the newly
645 developed retrieval algorithm, GEMS can be used to monitor aerosol vertical
646 information with high temporal and spatial resolution. To ensure significant sensitivity
647 of AEH retrieval, only AEH retrieval results are with AOD larger than 0.3 were shown.
648 For dust plumes over East Asia, AEH indicated significant aerosol vertical
649 information and insignificant diurnal variation in regions with severe dust plumes. After
650 spatial and temporal colocation, the AEH from GEMS aligned well with the AEH
651 information obtained from CALIOP. The differences in AEH between GEMS and
652 CALIOP for dust plume cases were -0.07 ± 1.09 and -0.11 ± 1.27 km, with 53.8% and
653 72.9% of all pixels showing differences less than 1.0 and 1.5 km, respectively. Large
654 AEH uncertainty was found mostly over inland China due to uncertainty in surface
655 reflectance and AOD over the land surface. In addition, AEH from GEMS was
656 overestimated compared to the TROPOMI ALH results due to different definitions of
657 ALH from TROPOMI and AEH from GEMS.
658 In long-term intercomparison with CALIOP, the average AEH difference was
659 estimated to be -0.03 km, with variation of around 1.4 km based on the standard
660 deviation for AOD > 0.4. In terms of sensitivity to surface albedo, the mean differences
661 were estimated to be 1.09 and 0.91 km over the ocean and land, respectively, which is
662 an insignificant difference of the biases between these two surface types. The large
663 variation in AEH difference between GEMS and CALIOP was caused by uncertainty in
664 the input parameters estimated from L2AERAOD and L2SFC. In the long-term
665 intercomparison with TROPOMI, this difference was significantly dependent on both

SSA and TYPE. The difference was 0.78 ± 0.81 km and 1.16 ± 0.92 km for pixels with SSA < 0.90 and 0.90 < SSA < 0.95, respectively. In addition, differences of 0.73 ± 0.77 and 1.34 ± 0.94 km were obtained for the "Absorbing" and the "Dust" types of aerosol, respectively. The AEH difference ranged from -0.23 ± 1.45 km (07:00 UTC, Number of Data = 867) to 1.01 ± 1.96 km (03:00 UTC, Number of Data = 23), showing diurnal dependence. The spatial difference in dominant aerosol type may impact the diurnal variation in AEH difference.

The case studies and results of the long-term validation show that AEH retrieved from GEMS can provide information on aerosol vertical distribution, with applications in diverse research fields. In particular, AEH information can be applied to AMF calculation for trace gases to consider the change in scattering weight change due to the presence of an aerosol layer. In addition, AEH considerably affects the surface particulate matter (PM) concentration obtained from satellite-based AOD because PM estimation is significantly affected by the mixing layer height of aerosols.

Although several fields of study may apply the AEH retrieval results, ~~uncertainty~~ retrieval uncertainty in AEH remains~~, driving large deviations in some pixels~~ due to the uncertainty of retrieved AOD and SSA. In addition, the uncertainty in surface reflectance and the discrepancy in O_2-O_2 SCD values between the simulation results and observations can be affected to the potential error sources of AEH from GEMS. Moreover, AEH provides representative layer height information as only one variable because of its sole reliance on O_2-O_2 SCD for direct estimation of aerosol height information. This method is limited to the consideration of aerosol vertical structures (i.e., Gaussian or exponential vertical distribution structures). Rather than using the GEMS sensor alone, using another absorption band for oxygen-based materials would

690 provide additional scattering information about aerosols.

691

692 **Acknowledgements**

693 This work was supported by the National Institute of Environment Research of the

694 Republic of Korea under Grant NIER-2023-04-02-050.

695

References

Accarreta, J. R., de Haan, J. F., and Stammes, P.: Cloud pressure retrieval using the O2-O2 absorption band at 477 nm, J. Geophys. Res., 109, D05204, doi:10.1029/2003JD003915, 2004

Ahn, C., Torres, O., and Jethva, H.: Assessment of OMI near-UV aerosol optical depth over land, J. Geophys. Res., 119, 2457-2473, 2014.

Bogumil, K., Orphal, J., Burrows, J. P., and Flaud, J. M.: Vibrational progressions in the visible and near-ultraviolet absorption spectrum of ozone, Chem. Phys. Lett., 349, 241-248, 2001.

Buchard, V., de Silva, A. M., Colarco, P. R., Darmenov, A., Randles, C. A., Govindaraju, R., Torres, O., Campbell, J., and Spurr, R.: Using the OMI aerosol index and absorption aerosol optical depth to evaluate the NASA MERRA Aerosol reanalysis, Atmos. Chem. Phys., 15, 5743-5760, 2015.

Chen, X., Wang, J., Xu, X., Zhou, M., Zhang, H., Garcia, L. C., Colarco, P. R., Janz, S. J., Yorks, J., McGill, M., Reid, J. S., de Graaf, M., and Kondragunta, S.: First retrieval of absorbing aerosol height over dark target using TROPOMI oxygen B band: Algorithm development and application for surface particulate matter estimates, Remote Sens. Env., 265, 112674, 2021.

Chimot, J., Veefkind, J. P., Vlemmix, T., de Haan, J. F., Amiridis, V., Proestakis, E., Marinou, E., and Levelt, P. F.: An exploratory study on the aerosol height retrieval from OMI measurements of the 477 nm O2-O2 spectral band using a neural network approach, Atmos. Meas. Tech., 10, 783-809, 2017.

Choi, H., Liu, X., Abad, G. G., Seo, J., Lee, K. -M., and Kim, J.: A fast retrieval of cloud parameters using a Triplet of wavelengths of oxygen dimer band around 477 nm, Remote Sens., 13, 152, doi: 10.3390/rs13010152, 2021.

Choi, W., Lee, H., Kim, J., Ryu, J. -Y., Park, S. S., Park, J., and Kang, H.: Effects of spatiotemporal O4 column densities and temperature-dependent O4 absorption cross-section on an aerosol effective height retrieval algorithm using the O4 air mass factor from the ozone monitoring instrument, Remote Sens. Env., 229, 223-233, 2019.

Choi, W., Lee, H., and Kim, J.: First TROPOMI retrieval of aerosol effective height using O4 absorption band at 477 nm and aerosol classification, IEEE Trans. Geosci., Remote Sens., 59, 9873-9886, 2021.

de Graaf, M., Stammes, P., Torres, O., and Koelemeijer, R. B. A.: Absorbing aerosol index: Sensitivity analysis, application to GOME and comparison with TOMS, J. Geophys. Res., 110, D01201, doi:10.1029/2004JD005178, 2005.

de Graaf, M., de Haan, J. F., and Sanders, A. F. J.: TROPOMI ATBD of the Aerosol Layer Height, 75pp, Royal Netherlands Meteorological Institute, Netherland.

Ding, S., Wang, J., and Xu, X.: Polarimetric remote sensing in oxygen A and B bands: Sensitivity study and information content analysis for vertical profile of aerosols, Atmos. Meas. Tech, 9, 2077-2092, 2016.

Dubuisson, P., Frouin, R., Dessaily, D., Duforet, L., Leon, J. –F., Voss, K., and Antoine, D.: Estimating the altitude of aerosol plumes over the ocean from reflectance ratio measurements in the O2 A-band, Remote Sens. Environ., 113, 1899-1911, doi:10.1016/j.rse.2009.04.018, 2009.

Gao, Y., Zhao, C., Liu, X., Zhang, M., and Leung, L. R.: WRF-Chem simulations of aerosols and anthropogenic aerosol radiative forcing in East Asia, Atmos. Environ., 92, 250-266, 2014.

Geddes, A., and Boesch, H.: Tropospheric aerosol profile information from high-resolution oxygen A-band measurements from space, Atmos. Meas. Tech., 8, 859-874, 2015.

Go, S., Kim, J., Park, S. S., Kim, M., Lim, H., Kim, J. -Y., Lee, D. -W., and Im, J.: Synergistic use of hyperspectral UV-visible OMI and broadband meteorological imager MODIS data for a merged aerosol product, Remote Sens., 12, 3987, doi:10.3390/rs12233987, 2020.

Griffin, D., Sioris, C., Chen, J., Dickson, N., Kovachik, A., de Graaf, M., Nanda, S., Veefkind, P., Dammers, E., McLinden, C. A., Makar, P., and Akingunola, A.: The 2018 fire season in North America as seen by TROPOMI: aerosol layer height intercomparisons and evaluation of model-derived plume heights, Atmos. Meas. Tech., 13, 1427-1445, 2020.

Herman, J. R., Bhartia, P. K., Torres, O., Hsu, C., Seftor, C., and Celarier, E.: Global distribution of UV-absorbing aerosols from Nimbus-7/TOMS data, J. Geophys. Res., 102(D14), 16911-16922, 1997.

Hong, H., Lee, H., Kim, J., Jeong, U., Ryu, J., and Lee, D. S.: Investigation of simultaneous effects of aerosol properties and aerosol peak height on the air mass factors for space-borne NO2 retrievals, Remote Sens., 9, 208, doi:10.3390/rs9030208, 2017.

Joiner, J., and Bhartia, P. K.: The determination of cloud pressures from rotational Raman scattering in satellite backscatter ultraviolet measurements, J. Geophys. Res., 100, 23019-23026, 1995.

Joiner, J., and Vasilkov, A. P.: First results from the OMI rotational Raman scattering cloud pressure algorithm, IEEE Trans. Geosci. Remote Sens., 44, 1272-1282, 2006.

Kim, M., Kim, J., Torres, O., Ahn, C., Kim, W., Jeong, U., Go, S., Liu, X., Moon, K. J., and Kim D. -R.: Optimal estimation-based algorithm to retrieve aerosol optical properties for GEMS measurements over Asia, 10, 162, doi:10.3390/rs10020162, 2018.

Kim, J., Jeong, U., Ahn, M. -H., Kim, J. H., Park, R. J., Lee, H., Song, C. H., Choi, Y. -S., Lee, K. -H., Yoo, J. -M., Jeong, M. -J., Park, S. K., Lee, K. -M., Song, C. -K., Kim, S. -W., Kim, Y. J., Kim, S. -W., Kim, M., Go, S., Liu, X., Chance, K., Chan Miller, C., Al-Saadi, J., Veihelmann, B., Bhartia, P. K., Torres, O., González Abad, G., Haffner, D. P., Ko, D. H., Lee, S. H., Woo, J. -H., Chong, H., Park, S. S., Nicks, D., Choi, W. J., Moon, K. -J., Cho, A., Yoon, J., Kim, S. -K., Hong, H., Lee, K., Lee, H., Lee, S., Choi, M., Veefkind, P., Levelt, P. F., Edwards, D. P., Kang, M., Eo, M., Bak, J., Baek, K., Kwon, H. -A., Yang, J., Park, J., Han, K. M., Kim, B. -R., Shin, H. -W., Choi, H., Lee, E., Chong, J., Cha, Y., Koo, J. -H., Irie, H., Hayashida, S., Kasai, Y., Kanaya, Y., Liu, C., Lin, J., Crawford, J. H., Carmichael, G. R., Newchurch, M. J., Lefer, B. L., Herman, J. R., Swap, R. J., Lau, A. K. H., Kurosu, T. P., Jaross, G., Ahlers, B., Dobber, M., McElroy, C. T., and Choi, Y.: New era of air quality from Space: Geostationary Environment Monitoring Spectrometer (GEMS), Bul. Ame. Meteorol. Soc., 101(1), E1–E22, 2020.

786 Kokhanovsky, A. A., and Rozanov, V. V.: The determination of dust cloud altitudes from
787 a satellite using hyperspectral measurements in the gaseous absorption band, Int. J.
788 Rem. Sens., 31, Nos. 9-10, 2729-2744, 2010.
789 Kooreman, M. L., Stammes, P., Trees, V., Sneep, M., Tilstra, L. G., de Graaf, M.,
790 Zweers, D. C. S., Wang, P., Tuinder, O. N. E., and Veefkind, J. P.: Effects of cloud
791 on the UV absorbing aerosol index from TROPOMI, Atmos. Meas. Tech., 13,
792 6407-6426, 2020.
793 Lorente, A., Boersma, K. F., Yu, H., Doerner, S., Hilboll, A., Richter, A., Liu, M.,
794 Lamsal, L. N., Barkley, M., De Smedt, I., Van Roozendael, M., Wang, Y., Wagner,
795 T., Beirle, S., Liu, J. -T., Krotkov, N., Stammes, P., Wang, P., Eskes, H. J., and Krol,
796 M.: Structural uncertainty in air mass factor calculation for NO2 and HCHO
797 satellite retrieval, Atmos. Meas. Tech., 10, 759-782, 2017.
798 Nanda, S., de Graaf, M., Sneep, M., de Haan, J. F., Stammes, P., Sanders, A. F. J.,
799 Tuinder, O., Veefkind, J. P., and Levelt, P. F.: Error sources in the retrieval of
800 aerosol information over bright surfaces from satellite measurements in the oxygen
801 A band, Atmos. Meas. Tech., 11, 161–175, https://doi.org/10.5194/amt-11-161-
802 2018, 2018.
803 Nanda, S., de Graaf, M., Veefkind, J. P., Sneep, M., ter Linden, M., Sun, J., and Level, P.
804 F.: A first comparison of TROPOMI aerosol layer height (ALH) to CALIOP data,
805 Atmos. Meas. Tech., 13, 3043-3059, 2020.
806 National Institute of Environmental Research, Geostationary Environment Monitoring
807 Spectrometer (GEMS) Algorithm Theoretical Basis Document: Aerosol Retrieval
808 Algorithm, 42pp, Ministry of Environment, Korea, 2020a.
809 National Institute of Environmental Research, Geostationary Environment Monitoring
810 Spectrometer (GEMS) Algorithm Theoretical Basis Document: Surface
811 Reflectance Algorithm, 35pp, Ministry of Environment, Korea, 2020b.
812 Park, S. S., Kim, J., Lee, H., Torres, O., Lee, K. –M., and Lee, S. D.: Utilization of O4
813 slant column density to derive aerosol layer height from a space-borne UV-visible
814 hyperspectral sensor: Sensitivity and case study, Atmos. Chem. Phys., 16, 1987-
815 2006, doi:10.5194/acp-16-1987-2016, 2016.

816 Park, S. S., Takemura, T., and Kim, J.: Effect of temperature-dependent cross sections
817 on O4 slant column density estimation by a space-borne UV-visible hyperspectral
818 sensor, Atmos. Environ., 152, 98-110, 2017.
819 Peng, J., Hu, M., Guo, S., Du, Z., Zheng, J., Shang, D., Zamora, M. L., Zeng, L., Shao,
820 M., Wu, Y. -S., Zheng, J., Wang, Y., Glen, C. R., Collins, D. R., Molina, M. J., and
821 Zhang R.: Markedly enhanced absorption and direct radiative forcing of black
822 carbon under polluted urban environments, Proc. Natl. Acad. Sci., 113, 4266-4271,
823 2016.
824 Penning de Vries, M. J. M., Beirle, S., and Wagner, T.: UV aerosol indices from
825 SCIAMACHY: Introducing the Scattering Index (SCI), Atmos. Chem. Phys., 9,
826 9555-9567, 2009.
827 Penning de Vries, M. J. M., Beirle, S., Hoermann, C., Kaiser, J. W., Stammes, P., Tilstra,
828 L. G., Tuinder, O. N. E., and Wagner, T.: A global aerosol classification algorithm
829 incorporating multiple satellite data sets of aerosol and trace gas abundances,
830 Atmos. Chem. Phys., 15, 10597-10618, 2015.
831 Prospero, J. M., Ginoux, P., Torres, O., Nicholson, S. E., and Gill T. E.: Environmental
832 characterization of global sources of atmospheric soil dust identified with the
833 Nimbus 7 total ozone mapping spectrometer (TOMS) absorbing aerosol product,
834 Rev. Geophys., 40, 1002, doi:10.1029/2000RG000095, 2002.
835 Qin, W., Fasnacht, Z., Haffner, D., Vasilkov, A., Joiner, J., Krotkov, N., Fisher, B., and
836 Spurr, R.: A geometry-dependent surface Lambertian-equivalent reflectivity
837 product for UV-vis retrievals – Part 1: Evaluation over land surfaces using
838 measurements from OMI at 466 nm, Atmos. Meas. Tech., 12, 3997-4017, 2019.
839 Rana, A., Jia, S., and Sarkar, S.: Black carbon aerosol in India: A comprehensive review
840 of current status and future prospects, Atmos. Res., 218, 207-230, 2019.
841 Sanders, A. F. J., de Haan, J. F., Sneep, M., Apituley, A., Stammes, P., Vieitez, M. O.,
842 Tilstra, L. G., Tuinder, O. N. E., Koning, C. E., and Veefkind, J. P.: Evaluation of
843 the operational Aerosol Layer Height retrieval algorithm for Sentinel-5 Precursor:
844 application to O2 A band observations from GOME-2A, Atmos. Meas. Tech., 8,
845 4947-4977, 2015.
846 Sanders, A. F. J. and de Haan, J. F.: TROPOMI ATBD of the Aerosol Layer Height
847 product, available at: http://www.tropomi.eu/sites/default/files/files/S5P-KNMI-

L2-0006-RP-TROPOMI_ATBD_Aerosol_Height-v1p0p0-20160129.pdf (last access: 8 June 2020), 2016.

Sanghavi, S., Martonchik, J. V., Landgraf, J., and Platt, U.: Retrieval of optical depth and vertical distribution of particulate scatterers in the atmosphere using O2 A- and B-band SCIAMACHY observations over Kanpur: A case study, Atmos. Meas. Tech., 5, 1099-1119, 2012.

Spurr, R. "User's Guide VLIDORT Version 2.6, RT Solutions.", Cambridge, MA, USA, 2013.

Thalman, R., and Volkamer, R.: Temperature dependent absorption cross-sections of O2-O2 collision pairs between 340 and 630 nm and at atmospherically relevant pressure. Phys. Chem. Chem. Phys. 15, 15371e15381, 2013.

Torres, O., Bhartia, P. K., Herman, J. R., Ahmad, Z., and Gleason, J.: Derivation of aerosol properties from satellite measurements of backscattered ultraviolet radiation: Theoretical basis, J. Geophys. Res., 103(14), 17099-17110, 1998.

Torres, O., Decae, R., Veefkind, P., and de Leeuw, G.: OMI Aerosol Retrieval Algorithm, OMI Algorithm Theoretical Basis Document, Vol. III, Clouds, Aerosols and Surface UV Irradiance, NASA-KNMI ATBD-OMI-03, pp. 47-71, 2002.

Torres, O., Jethva, H., Ahn, C., Jaross, G., and Loyola, D. G.: TROPOMI aerosol products: evaluation and observations of synoptic-scale carbonaceous aerosol plumes during 2018-2020, Atmos. Meas. Tech., 13, 6789-6806, 2020.

Vandaele, A. C., Hermans, C., Simon, P. C., Carleer, M., Colin, R., Fally, S., Merienne, M. F., Jenouvrier, A., and Coquart, B.: Measurements of the NO2 absorption cross-section from 42000 cm-1 to 10000 cm-1 (238-1000 nm) at 220 K and 294 K, J. Quant. Spectrosc. Radiat. Transfer, 59, 3-5, 171-184, 1998.

Vasilkov, A., Joiner, J., Spurr, R., Bhartia, P. K., Levelt, P., and Stephens, G.: Evaluation of the OMI cloud pressures derived from rotational Raman scattering by comparisons with other satellite data and radiative transfer simulations, J. Geophys. Res., 113, D15S19, doi:10.1029/2007JD008689, 2008.

Vasilkov, A., Yang, E. -S., Marchenko, S., Qin, W., Lamsal, L., Joiner, J., Krotkov, N., Haffner, D., Bhartia, P. K., and Spurr, R.: A cloud algorithm based on the O2-O2 477 nm absorption band featuring an advanced spectral fitting method and the use

879 of surface geometry-dependent Lambertian-equivalent reflectivity, Atmos. Meas.
880 Tech., 11, 4093-4107, 2018.
881 Wang, R., Tao, S., Wang, W., Liu, J., Shen, H., Shen, G., Wang, B., Liu, X., Li, W.,
882 Huang, Y., Zhang, Y., Lu, Y., Chen, H., Chen, Y., Wang, C., Zhu, D., Wang, X., Li,
883 B., Liu, W., and M, J.: Black carbon emissions in China from 1949 to 2050,
884 Environ., Sci. Technol., 46, 7595-7603, 2012.
885 Winker, D. M., Vaughan, M. A., Omar, A. H., Hu, Y., Powell, K. A., Liu, Z., Hunt, W.
886 H., and Young, S. A.: Overview of the CALIPSO mission and CALIOP data
887 processing algorithms, J. Atmos. Oceanic Technol., 26, 2310-2323, 2009.
888 Zeng, Z. -C., Chen, S., Natraj, V., Le, T., Xu, F., Merrelli, A., Crisp, D., Sander, S. P.,
889 and Yung, Y. L.: Constraining the vertical distribution of coastal dust aerosol using
890 OCO-2 O2 A-band measurements, Remote Sens. Env., 236, 111494, 2020.
891